THE ASTROPHYSICAL JOURNAL, 338:654–676, 1989 March 15

LARGE PECULIAR VELOCITIES IN THE HYDRA-CENTAURUS SUPERCLUSTER

M. AARONSON,[1, 2, 3] G. D. BOTHUN,[4] M. E. CORNELL,[1, 3] J. A. DAWE,[5] R. J. DICKENS,[6]
P. J. HALL,[7] HAN MING SHENG,[3, 8] J. P. HUCHRA,[9] J. R. LUCEY,[10] J. R. MOULD,[3, 8, 11]
J. D. MURRAY,[12] R. A. SCHOMMER,[13] AND A. E. WRIGHT[12]

Received 1988 July 7; accepted 1988 August 29

ABSTRACT

Distances from the infrared Tully-Fisher relation have been obtained with the Parkes radio telescope for six clusters of galaxies in the Hydra-Centaurus supercluster. One of these clusters is Pavo, a possible extension of the supercluster on the south side of the galactic plane. Three of these clusters show significant positive peculiar velocities of order 500 km s^{-1} in a comoving reference frame in which the observer is at rest with respect to the cosmic microwave background radiation. The net peculiar velocity of the sample suggests that Hydra-Centaurus tends to share the motion of the Local Group in this reference frame. When added to the Arecibo cluster sample, the data also fit a model in which two mass concentrations, one at Virgo and one just beyond the centroid of the Parkes sample, perturb the Hubble flow. A full model of the gravitational field in the sample volume based on the distribution of *IRAS* galaxies provides a better fit to the data without requiring a mass distribution different from the distribution of galaxies. Despite the significance of the peculiar velocities of some clusters, the present sample can only put an upper limit on the rms one-dimensional peculiar velocities in the population of gravitationally perturbed clusters from which it is drawn. This upper limit is $v_{pec}(\mathrm{rms}) < 400$ km s^{-1}. These measurements of peculiar velocities remain consistent with the expectations for a universe dominated by cold dark matter, although the coherence length of the Virgo-Hydra-Centaurus flow is an uncomfortable constraint.

Subject headings: cosmology — galaxies: clustering — galaxies: redshifts — radio sources: galaxies — radio sources: 21 cm radiation

I. INTRODUCTION

In a coordinate system moving with the Hubble expansion, any finite velocity is a "peculiar velocity." If we assume that the source of these velocities is gravity, the study of peculiar velocities can, in principle, provide a unique picture of the mass distribution in the universe. There are two other key indicators of large-scale structure. The first is various statistical measures of the clustering of galaxies. The second is the lumpiness of the microwave background radiation. Both of these are measures of the *light* distribution, which is widely suspected to cluster differently from the *mass*.

The difficulty with the measurement of peculiar velocities is that one needs to measure distances to galaxies. Fortunately, for this purpose relative distances will suffice. Absolute distances remain problematical, pending the measurement of Cepheid variables, for example, in distant galaxies (see, e.g., Aaronson and Mould 1986).

We know that peculiar velocities exist on large scales, because a Virgocentric flow pattern has been shown to provide a basic description of the kinematics of galaxies within the Local Supercluster (Peebles 1976; Aaronson *et al.* 1982; Tonry and Davis 1981; Davis and Peebles 1983; Kraan Korteweg 1986). Furthermore, the Local Supercluster itself exhibits a bulk motion in a reference frame composed of clusters of galaxies in the distance interval (50, 100) h^{-1} Mpc. (Here h is the value of the Hubble constant in units of 100 km s^{-1} Mpc^{-1}.) Aaronson *et al.* (1986) showed that the vector sum of the Local Group's Virgocentric motion and the Local Supercluster's bulk motion were indistinguishable within the errors of the reflex motion analysis from the Local Group motion relative to the cosmic microwave background.

Shaya (1984) and Tammann and Sandage (1985) were first to point out that the source of this large peculiar velocity of the Local Supercluster might be the neighboring Hydra-Centaurus supercluster. An all-sky survey of elliptical galaxies, however, suggested that, rather than providing the source of the flow, galaxies in Hydra and Centaurus were participating in it (Dressler *et al.* 1987). Lynden-Bell *et al.* (1988) fitted these data as a flow toward a "great attractor" situated beyond Hydra-Centaurus and coincident with a large and previously nameless concentration of galaxies.

Previous work by Aaronson *et al.* (1986), employing the infrared Tully-Fisher relation (IRTF) to measure the necessary relative distances outside the Local Supercluster, was confined to the declination range of the Arecibo telescope. Recent advances in receiver technology at the Parkes radio telescope of the Australian National Radio Astronomy Observatory have permitted study of galaxies as distant as Hydra-Centaurus at 21 cm. In this paper we report work on six clusters of galaxies in and around Hydra-Centaurus to probe the kinematics of this interesting region. The data are consistent with the "great attractor" model, but also with a more natural model in which peculiar velocities are predicted from the net

[1] Steward Observatory, University of Arizona.
[2] Deceased, 1987 April 30.
[3] Visiting Astronomer at Cerro Tololo Inter-American Observatory, which is operated by AURA, Inc., under contract with the National Science Foundation.
[4] University of Michigan.
[5] Australian National University.
[6] Rutherford Appleton Laboratory.
[7] University of Sydney.
[8] Palomar Observatory, California Institute of Technology.
[9] Harvard Smithsonian Center for Astrophysics.
[10] Anglo Australian Observatory and University of Durham.
[11] Guest Investigator at the Las Campanas Observatory of the Carnegie Institution of Washington.
[12] Australian National Radio Astronomy Observatory.
[13] Rutgers University.

TABLE 1

MEAN REDSHIFTS OF THE CLUSTER SAMPLE

Cluster	l	b	Radius	Velocity Range[a]	Mean Velocity[b]
Antlia	273	20	4°	2000 to 3600	2948 ± 84
NGC 3557	282	22	4	2600 to 3200	2973 ± 79
Hydra	269.6	26.5	4	1700 to 5600	3722 ± 85
Cen 30	302.5	21.5	3	1700 to 4100	3041[b] ± 52
Cen 45	302.5	21.5	3	4100 to 5600	4570[b] ± 35
ESO 508	309.2	39.2	4	2200 to 3800	2903 ± 60
Pavo	324.4	−34	4	2800 to 5000	3798 ± 123

[a] Heliocentric velocities in km s^{-1}.
[b] From Lucey, Currie, and Dickens 1986*a*.

gravitational acceleration of a complete sample of galaxies in the local 100 h^{-1} Mpc radius (Yahil 1988; Strauss and Davis 1988*a*).

II. 21 CENTIMETER OBSERVATIONS

We began this program at Parkes in 1979, obtaining a few detections of galaxies in the Antlia, NGC 3557, and Centaurus clusters, identified in the southern redshift survey of Sandage (1975). Development of a dual polarization receiver with a system temperature of 40 K in 1986 made it possible to obtain substantial samples of galaxies in these clusters, and four further clusters were added to the list: Hydra I = Abell 1060, ESO 508, Telescopium, and Pavo (Hopp and Materne 1985; Sandage 1975). The mean redshifts of these clusters have been determined from the catalog of Huchra (1988), using the search parameters given in Table 1. After a run of nondetections (see below) we abandoned the Telescopium cluster, leaving a total of six useful clusters.

The sample was drawn from a diameter-limited catalog (Lauberts 1982). Most of the suitably inclined galaxies later than S0/a, larger than 2′ major axis diameter, and within a defined cluster radius were observed. At 1.5 the fraction observed falls to one-half, except in Pavo, where this cut-off occurs at 1′.

Most of the galaxies were observed with the Parkes 64 m telescope during 1987 February. Used in conjunction with a wide-band horn feed centered at 1420 MHz, the telescope has a half-power beamwidth of 15′ and a sensitivity of 0.63 K Jy^{-1}. During our observations the Parkes 1024-channel one-bit autocorrelation spectrometer (Ables *et al.* 1975) was configured to produce two overlapping 10 MHz (256-channel) band segments for each polarization. This resulted in a velocity coverage of 4000 km s^{-1} and a raw velocity resolution of 8.3 km s^{-1}. The center velocity was chosen to correspond to the mean cluster velocity of the galaxy under investigation, or the velocity of the galaxy itself, where that was known. Each galaxy was observed for 5 or 10 minutes, after which a portion of blank sky offset from the source by an equal time in R.A. was observed for the same integration time. The total-intensity (polarization added) spectra resulting from pairs of such observations were averaged, then Hanning smoothed. A linear or quadratic baseline was fitted to those portions of the spectrum outside the H I profile and has been subtracted from Figure 1*a*.

Figure 1*b* shows profiles of galaxies observed solely in the 1979 to 1983 period, before the advent of the SPECTRA data reduction package. Velocity widths for these galaxies were measured graphically. Ten galaxies from this early period were reobserved in 1987. Their velocity widths show no systematic differences and have been averaged with the more recent data.

Positions for the galaxies, and names for those not to be found in the NGC or IC, were taken from Lauberts (1982). The pointing of the telescope was checked daily and found to be good to 30″. Frequent flux density calibrations were performed using the sources PKS 0915−118 (Hydra A) and PKS 1934−638 as references. Flux densities of 43.5 Jy and 16.0 Jy, respectively, were assumed, and we estimate the errors in the 21 cm flux density determination are no greater than 10% of the values shown in the neutral hydrogen profiles of Figure 1.

Redshifts and velocity widths defined according to the precepts of Aaronson, Mould, and Huchra (1980) are given in Table 2. Column (4) gives the profile width at 20% peak intensity, and the next two columns give the uncertainties in this measurement. These errors were calculated by perturbing the 20% level by the rms noise in the spectrum, yielding an uncertainty in the sense of lower velocity width (column [5]) and of higher velocity width (col. [6]). In a few cases where the entry in column (6) exceeded 100 km s^{-1}, it was replaced by an estimate based on increasing ΔV_{50} by 10% (see Aaronson *et al.* 1980; Fig. 1). Note that this is a redefinition of the estimated *uncertainty*, not of the velocity width itself. Columns (7), (8), and (9) give the corresponding quantities for the profile width at 50% peak intensity. The redshift of the galaxy is given in column (12) corrected to the Local Group centered reference frame by $+300 \sin l \cos b$ km s^{-1}. The signal-to-noise ratio is recorded in column (19) and the integrated H I flux in column (20). A list of nondetections is provided in Table 3, which also records our observations in the Telescopium cluster.

The first zero of the 64 m beam is at 15′ radius at this frequency with negligible sidelobes beyond that radius. However, this large beam can lead to confusion in rich clusters of galaxies. We rejected from the sample NGC 3347 and NGC 3358 at 10′ separation. Their profiles indicated a common redshift of 2950 km s^{-1} heliocentric and were probably confused. We also rejected 377−17, 12′ from NGC 3573 and apparently at the same redshift. In Centaurus the profile of 323−72 is clearly affected by confusion. A second, early-type galaxy 323−76 is 8′ away, but its heliocentric velocity is 3551 km s^{-1} (Dickens, Currie, and Lucey 1986). There is a third anonymous galaxy 5′ away, just a little smaller in size. Optical redshifts of these galaxies would solve this puzzle.

A small number of these galaxies have been observed before at 21 cm, and the comparison of measured quantities is given in Table 4. There is good overall agreement with previous data and with optical redshifts (Huchra 1988). Particularly important in the present context is the comparison of Parkes velocity widths with those from other sites. Three galaxies from Fisher and Tully (1981) yield ΔV_{20} (Parkes)/ΔV_{20}(FT) = 0.96 ± 0.07. Excluding 507−67 for which neither velocity widths nor fluxes

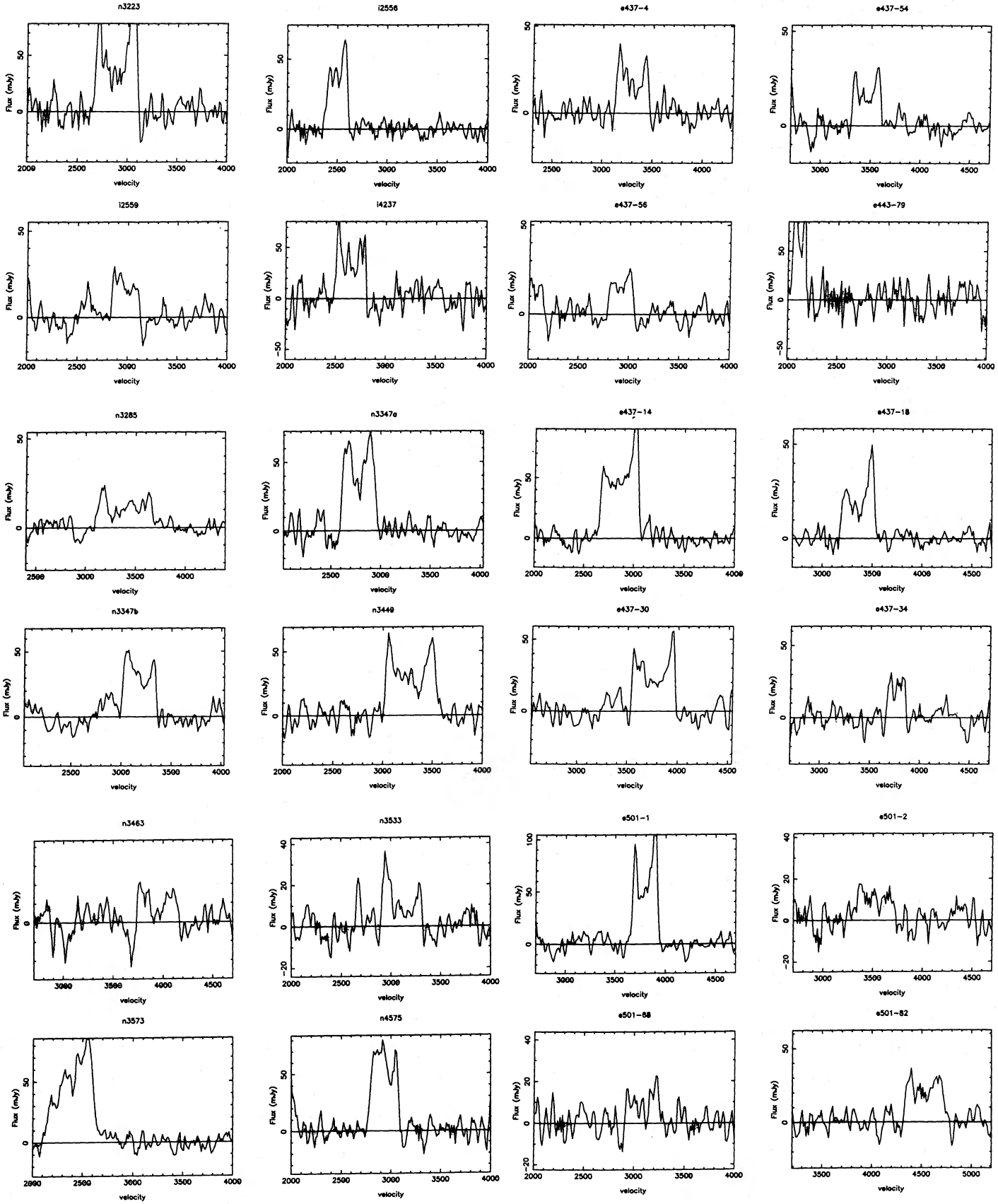

FIG. 1*a*.—Line profiles of galaxies at 21 cm. The velocity scale is heliocentric.

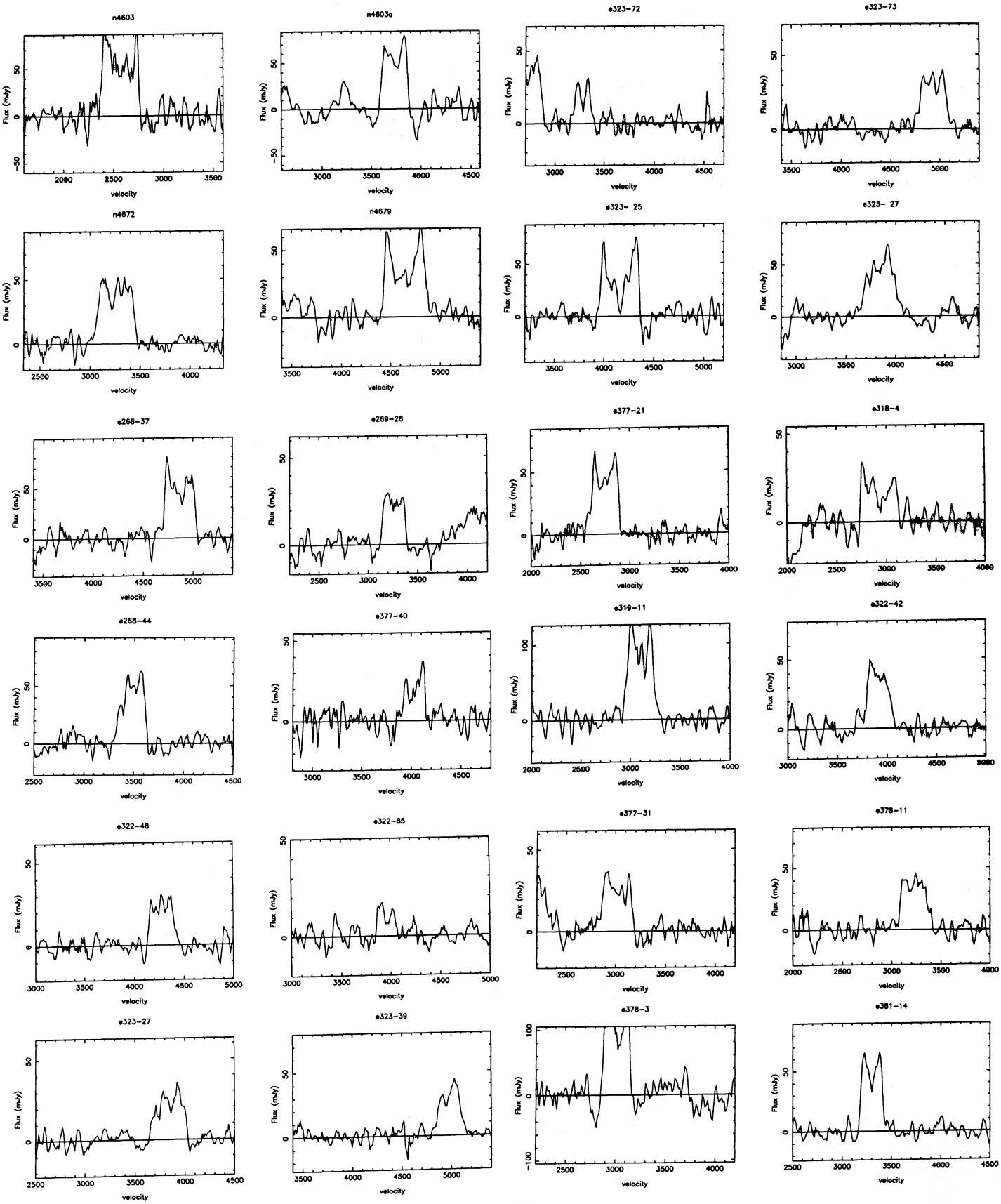

FIG. 1*a*—*Continued*

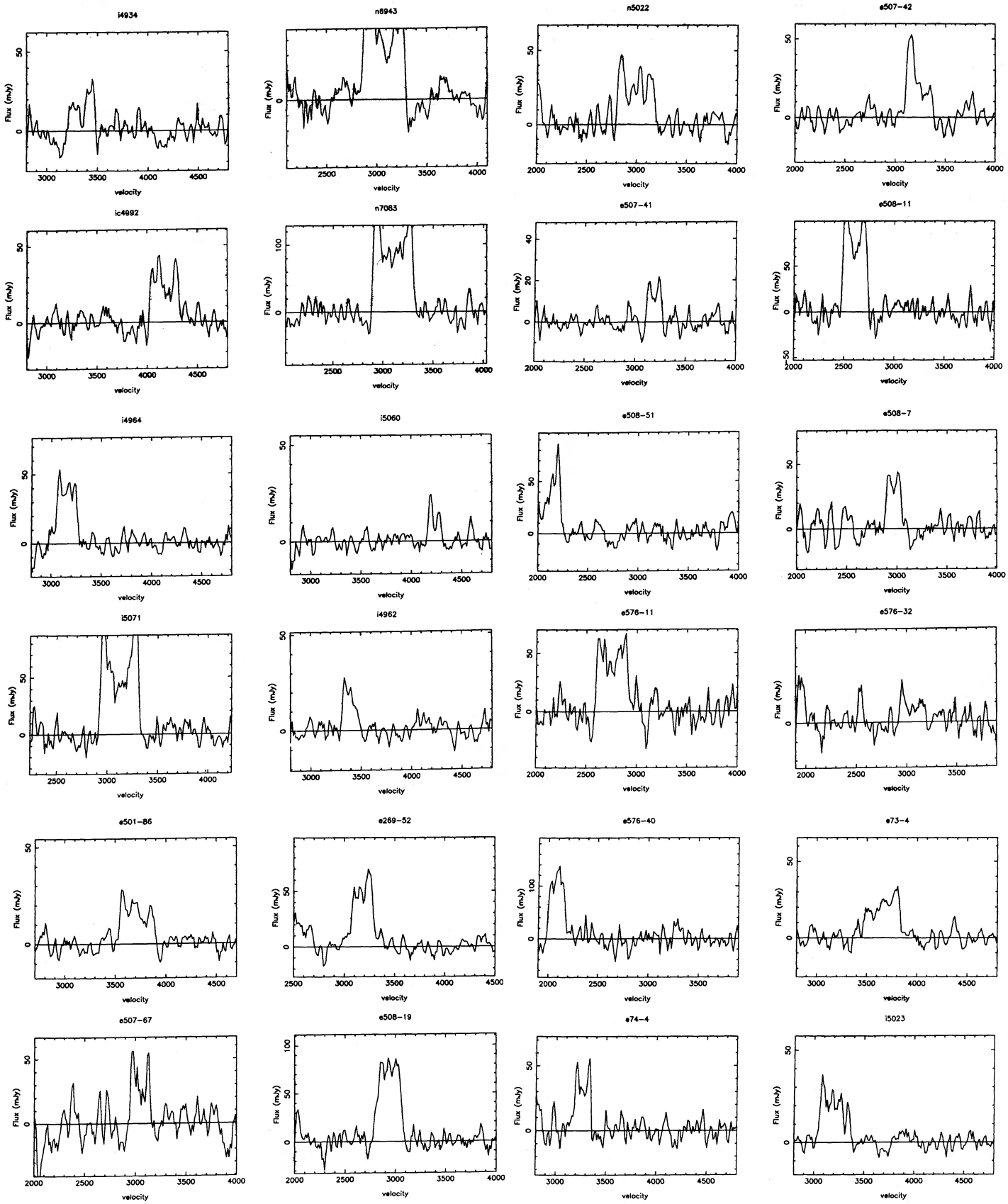

FIG. 1*a*—*Continued*

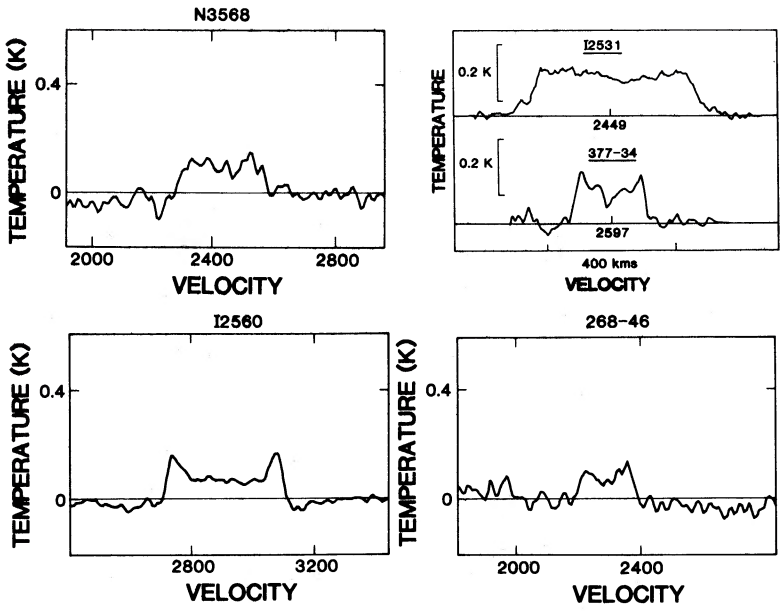

FIG. 1*b*

match, we obtain a mean ratio of 0.97 ± 0.02 for nine galaxies from Richter and Huchtmeier (1987). And five galaxies in Pegasus observed specifically for comparative purposes yield ΔV_{20}(Parkes)/ΔV_{20}(Arecibo) = 0.99 ± 0.02. Systematic errors in velocity widths can therefore be ruled out as a source of spurious peculiar velocities.

III. OPTICAL SURFACE PHOTOMETRY

Most of the galaxies were subsequently imaged with a CCD camera at the f/7.5 focus of the Swope 1 m telecope of the Las Campanas Observatory. The detector was an RCA CCD with a pixel spacing of 0.″86. Exposures of 900 s at *B* and 300 s at *V* were obtained for all objects under photometric conditions. A few of the galaxies were observed with a very similar CCD camera at the 0.9 m telescope of Cerro Tololo Inter-American Observatory.

The images were debiased and flat-fielded using dome flats in the usual way. Foreground stars in and around the galaxy images were masked, and elliptical isophotes were fitted in the manner described by Cornell *et al.* (1987). The resulting surface photometry was corrected for atmospheric extinction and the color term in the photometric transformations to yield an isophote at $B = 25$ mag s^2, the standard isophote of the *Second Reference Catalogue of Bright Galaxies* (RC2—de Vaucouleurs, de Vaucouleurs, and Corwin 1976). The isophotal diameter D_{25} is given in column (14) of Table 2 in the 0.1 units specified in the RC2. The axial ratio *R* follows in column (15). In one or two cases there is a colon following an entry, indicating uncertainty resulting from flat-fielding difficulties experienced in twilight observations. In several cases where photometry is available in the RC2, galaxies were not imaged, and the values in columns (14) and (15) are from the RC2, followed by an "R" in column (14).

Aaronson *et al.* (1987) adopted a formula by Mould and Ziebell (1982) to calculate D_{25} and *R* from eye-estimated major and minor axes by Lauberts (1982). The comparison of these transformed estimates and the new measurements is made in Figure 2. The rms scatter in the transformed ESO catalog estimates is 0.09 in log *D*, and there is an offset of 0.05, arising mostly from galaxies with log $D < 1.4$. There is also a suggestion of small systematic differences between different clusters. In eight cases where no CCD surface photometry is available, the Mould and Ziebell value is given in column (14) with an asterisk. We have applied no correction to these values, because they mostly occur in the Pavo cluster, where there is no independent evidence for any offset. Column (13) of Table 2 contains the major axis diameter corrected for inclination and for Galactic reddening following the cosecant formulation of Aaronson, Mould, and Huchra (1980). Multicolor CCD photometry of these galaxies will be discussed in a later paper.

IV. INFRARED PHOTOMETRY

Photometry at 1.6 μm was obtained for almost all the galaxies using photometers on the 1 m Swope (LC 40) and 2.5 m du Pont (C100) telescopes at Las Campanas Observatory. Some galaxies were also observed at the 1.5 m telescope (CT 60) of Cerro Tololo Inter-American Observatory. Observational techniques are described by Aaronson *et al.* (1982). Multiaperture *H* magnitudes corrected as indicated therein are recorded in Table 5. The column labeled "Obj" contains the telescope code (in parentheses above) identifying the origin of the observation. The column labeled "Ap" gives the diameter of the circular photometer aperture in arcseconds, and the *H* magnitude follows. The statistical uncertainty associated with these measurements is generally 0.03 mag; cases where the uncertainties are larger (0.05 to 0.1 mag) are indicated by a colon.

The multiaperture photometry was interpolated to the diameter log $D_1 - 0.5$, and corrected for reddening and redshift in accordance with equation (7) of Aaronson *et al.* (1980). The reddening correction here again is a simple cosecant law and always less than 0.05 mag. The resulting values are recorded in column (10) of Table 2 as $H^c_{-0.5}$. The error estimate in column (11) takes account of the scatter in the growth curve, where more than two measurements are available, and the range in

TABLE 2

OPTICAL AND 21 CENTIMETER PROPERTIES

Object	i	log	ΔV_{20}	±	ΔV_{50}	±	$H^c_{-0.5}$	±	v_0	log	log	log	Cluster	m-M	±	S/N	F_{HI}
	deg	$\Delta V(0)$	km/s		km/s		mag		km/s	D_1	D_{25}	R		mag			Jy km/s
(1)	(2)	(3)	(4)	(5) (6)	(7)	(8) (9)	(10)	(11)	(12)	(13)	(14)	(15)	(16)	(17)	(18)	(19)	(20)
N3223	55	2.736	451	-5 +13	411	-8 +12	8.55	0.03	2629	1.59	1.61R	0.20	Antlia	31.81	0.06	10.6	22.0
N3347A	76	2.571	365	-11+5	332	-10+6	10.57	0.10	2519	1.25	1.34	0.46	Antlia	32.38	0.14	12.3	17.0
N3347B	90	2.554	361	-13+11	335	-11+10	11.06	0.03	2922	1.46	1.59R	0.69	Antlia	32.69	0.15	6.4	12.1
N3449	67	2.775	556	-40+31	504	-6 +8	9.32	0.03	3032	1.36	1.42R	0.33	Antlia	32.88	0.19	8.4	19.2
IC2531	90	2.725	535	-34+34	492	-10+10	9.30	0.12	2190	1.69	1.82:	1.00	Out	32.49	* *	5	40.3
IC2556	65	2.420	240	-9 +5	206	-5 +6	12.28	0.03	2237	1.25	1.29	0.30	Antlia	32.38	0.15	12.0	9.5
IC2559	72	2.476	287	-7 +9	275	-21+9	11.20	0.03	2716	1.17	1.25	0.39	Antlia	31.98	0.14	5.0	5.3
IC2560	65	2.659	417		390		9.44	0.03	2632	1.53	1.57:	0.30	Antlia	32.08	0.03	8.0	49.8
318-4	86	2.587	389	-8 +10	369	-9 +12	10.39	0.04	2666	1.34	1.46	0.63	Antlia	32.36	0.11	6.5	6.8
437-14	71	2.625	402	-5 +6	379	-3 +4	9.99	0.03	2604	1.26	1.33	0.38	Antlia	32.32	0.06	18.1	22.1
437-18	85	2.544	352	-9 +11	327	-18+6			3118	1.08	1.20	0.61	NoPhot	* * *	* *	13.0	8.0
437-56	52	2.521	263	-16+14	240	-17+17	11.20	0.03	2665	1.18	1.20	0.17	Antlia	32.48	0.22	4.6	4.3
N3285	52	2.860	575	-34+2	533	-23+38	9.34	0.04	3161	1.37	1.39R	0.17	Hydra	33.44	0.08	4.7	6.9
N3463	67	2.662	427	-20+13	407	-34+20	10.83	0.03	3723	1.10	1.16	0.32	Hydra	33.50	0.14	3.3	4.3
437-4	54	2.605	330	-6 +24	315	-12+9	11.25	0.08	3056	1.17	1.20	0.19	Hydra	33.39	0.17	6.9	6.8
437-30	89	2.639	440	-8 +11	426	-7 +5	10.06	0.03	3515	1.37	1.50	0.67	Hydra	32.51	0.09	7.0	12.4
437-34	79	2.304	200	-13+12	183	-15+12	13.65	0.03	3530	0.96	1.06	0.51	Hydra	32.22	0.38	4.7	4.0
437-54	90	2.468	297	-6 +12	284	-8 +6	12.23	0.05	3227	1.02	1.16	0.80	Hydra	32.91	0.16	7.8	5.6
501-1	65	2.464	267	-6 +6	244	-3 +4	12.49	0.06	3576	1.21	1.27	0.30	Hydra	33.12	0.12	19.2	18.1
501-2	90	2.605	407	-42+ *	370	-39+ *	11.92	0.10	3292	0.96	1.09*	0.74	Low SN	34.06	* *	3.7	4.2
501-68	76	2.554	351	-23+36	325	-9 +15	11.47	0.04	2843	1.20	1.29	0.46	Hydra	33.10	0.37	4.7	3.3
501-82	66	2.651	414	-18+44	385	-20+17	11.22	0.03	4321	1.12	1.18:	0.31	Hydra	33.78	0.26	5.6	9.3
501-86	67	2.610	381	-29+9	341	-15+10	11.57	0.03	3492	1.19	1.26	0.33	Hydra	33.77	0.20	7.2	6.1
N3533	85	2.616	416	-9 +64	395	-11+13	9.93	0.07	2861	1.36	1.48	0.62	N3557	32.18	0.33	6.0	5.0
N3568	79	2.492	307		289		10.27	0.03	2153	1.28	1.38R	0.51	Fore	31.23	* *	6.0	32.2
N3573	68	2.738	511	-28+24	430	-92+22	9.51	0.07	2143	1.36	1.41	0.34	Fore	32.79	* *	13.0	26.4
319-11	58	2.564	312	-25+21	254	-6 +18	11.09	0.11	2852	1.36	1.39:	0.22	N3557	32.82	0.30	12.6	29.4
377-34	82	2.385	242		226		11.79	0.09	2329	1.25	1.36	0.56	Fore	31.45	* *	8.0	25.4
377-21	71	2.542	332	-20+10	267	-6 +6	11.32	0.05	2507	1.27	1.34	0.38	N3557	32.82	0.21	13.2	14.3
377-31	67	2.548	329	-15+22	292	-11+16	11.55	0.03	2770	1.23	1.29	0.33	N3557	33.11	0.24	8.2	8.2
377-40	76	2.366	228	-8 +26	212	-12+11	14.26	0.18	3764	0.84	0.93	0.45	Back	33.68	* *	5.5	4.9
378-3	64	2.484	277	-11+18	253	-6 +6	11.52	0.04	2775	1.23	1.28	0.29	N3557	32.39	0.24	9.7	34.8
378-11	90	2.512	328	-10+35	273	-16+25	12.30	0.03	2988	1.05	1.18	0.70	Back	33.48	* *	8.1	10.8
N4679	62	2.695	445	-21+23	415	-16+9	10.22	0.04	4470	1.32	1.36R	0.27	Cen45	33.16	0.16	9.3	17.7
268-37	60	2.581	334	-10+27	309	-5 +8	11.86	0.03	4687	1.14	1.17	0.24	Cen45	33.77	0.21	10.0	16.8
322-48	90	2.461	293	-19+25	250	-10+23	12.38	0.04	4083	1.08	1.21	0.68	Cen45	32.98	0.39	7.3	6.2
322-76	42	2.690	328	-13+25	308	-33+13			4364	1.07	1.09*	0.10	FaceOn	* * *	* *	4.4	13.1
323-25	70	2.628	405	-11+26	381	-7 +10	10.39	0.03	4043	1.26	1.33	0.37	Cen45	32.74	0.17	8.4	15.1
323-39	61	2.520	293	-23+83	230	-22+21	13.31	0.03	4811	0.98	1.02	0.25	Cen45	34.58	0.67	7.3	8.2
323-73	64	2.549	324	-31+16	269	-15+15	11.58	0.03	4777	1.07	1.12	0.29	Cen45	33.16	0.32	8.8	9.1
N4575	39	2.680	307	-11+14	274	-12+11	10.15	0.03	2742	1.34	1.34R	0.09	FaceOn	32.97	* *	10.6	17.7
N4603A	78	2.485	302	-17+16	263	-19+15	10.72	0.03	3536	1.20	1.29	0.49	Cen30	31.60	0.27	5.7	15.4
N4603	53	2.708	411	-17+12	361	-8 +7	9.32	0.03	2369	1.56	1.58R	0.18	Cen30	32.37	0.10	8.0	22.7
N4672	67	2.636	403	-11+17	356	-8 +18	10.32	0.03	3052	1.31	1.31	0.33	Cen30	32.75	0.13	13.1	15.6
268-44	68	2.509	303	-10+18	270	-33+7	11.28	0.06	3269	1.09	1.14	0.34	Cen30	32.42	0.21	11.2	13.2
268-46	81	2.319	207		188		12.61	0.20	2057	1.27	1.38	0.54	Cen30	31.38	0.20	3.0	17.3
269-28	74	2.440	267	-23+5	227	-4 +11	13.05	0.03	3059	1.00	1.08	0.42	Cen30	33.40	0.28	9.6	5.8
269-52	90	2.381	243	-11+11	208	-7 +10	13.69	0.03	2983	1.07	1.20	0.88	Out	33.31	* *	11.8	11.6
321-25	61	2.581	337		309		11.01	0.03	1900	1.30	1.35*	0.26	Out	32.92	* *	15.0	28.7
322-42	77	2.469	290	-33+15	235	-7 +14	12.08	0.08	3714	1.17	1.26	0.47	Cen30	32.77	0.45	10.4	9.4
322-85	79	2.337	216	-21+19	192	-20+19	13.01	0.05	3764	1.02	1.12	0.51	Cen30	32.04	0.55	4.3	2.3
323-27	62	2.613	368	-22+19	306	-16+38	10.81	0.04	3655	1.21	1.25	0.27	Cen30	33.03	0.21	7.3	7.7
323-72	77	2.276	186	-14+18	160	-13+17	12.82	0.07	3085	0.85	0.94	0.48	HSB	30.98	* *	5.2	3.8
381-14	90	2.388	247	-8 +11	223	-5 +4	12.86	0.05	3102	1.08	1.21	0.74	Cen30	32.57	0.22	14.0	12.1
N5022	88	2.587	390	-6 +8	367	-16+9	10.26	0.03	2847	1.24	1.38	0.66	E508	32.22	0.08	8.5	10.4
IC4237	46	2.628	309	-8 +16	293	-5 +9	10.47	0.03	2507	1.27	1.29R	0.13	E508	32.82	0.12	6.3	12.4
443-79	81	2.172	148	-8 +8	133	-5 +4	13.94	0.03	1935	1.07	1.19	0.55	Fore	30.53	* *	8.2	10.8

TABLE 2—*continued*

Object	i	log	ΔV_{20}	±	ΔV_{50}	±	$H^c_{-0.5}$	±	v_0	log	log	log	Cluster	m-M	±	S/N	F_{HI}
	deg	$\Delta V(0)$	km/s		km/s		mag		km/s	D_1	D_{25}	R		mag			Jy km/s
(1)	(2)	(3)	(4)	(5) (6)	(7)	(8) (9)	(10)	(11)	(12)	(13)	(14)	(15)	(16)	(17)	(18)	(19)	(20)
507-41	45	2.363	164	-10 +8	143	-13 +13	12.96	0.05	2989	0.94	0.96	0.12	Out	32.34	**	5.7	2.0
507-42	65	2.495	286	-16 +21	252	- * +18	11.42	0.08	3028	1.04	1.10	0.30	Out	32.41	**	6.5	7.2
507-67	41	2.488	205	-7 +8	188	-5 +8	11.54	0.03	2871	1.25	1.27	0.10	FaceOn	32.45	0.12	7.6	7.1
508-7	66	2.266	170	-12 +17	150	-9 +7	13.16	0.03	2803	1.12	1.19	0.31	E508	31.18	0.49	7.1	5.7
508-11	90	2.418	264	-6 +8	241	-13 +7	11.77	0.14	2424	1.36	1.50	0.78	E508	31.85	0.20	11.5	21.8
508-19	75	2.467	286	-9 +17	237	-12 +13	12.22	0.03	2778	1.16	1.26:	0.44	E508	32.90	0.22	13.0	18.8
508-51	63	2.188	138	-34 +41	126	-31 +38	13.13	0.03	1997	1.13	1.19	0.28	Fore	29.96	**	9.9	9.2
576-11	90	2.516	331	-8 +32	310	-12 +9	10.91	0.12	2606	1.35	1.49	0.77	E508	32.13	0.30	7.7	16.1
576-32	50	2.546	274	-18 +37	253	- * +20	10.90	0.03	2884	1.30	1.33	0.16	E508	32.46	0.34	3.7	2.5
576-40	90	2.264	185	-8 +11	160	-8 +10	12.39	0.03	1929	1.20	1.34	0.70	Fore	30.39	**	9.4	18.9
N6943	64	2.682	437	-9 +22	414	-9 +10	9.19	0.03	2996	1.55	1.61R	0.29	Pavo	32.02	0.12	8.0	41.6
N7083	54	2.711	421	-11 +14	394	-6 +8	8.84	0.03	3012	1.61	1.65R	0.19	Out	31.92	**	10.8	42.4
IC4934	83	2.430	270	-6 +19	259	-13 +8	12.62	0.03	3238	1.06	1.18*	0.57	Pavo	32.86	0.24	5.1	4.3
IC4962	89	2.255	182	-20 +25	152	-17 +14	14.99	0.03	3278	0.83	0.97	0.67	Pavo	32.85	0.80	5.4	2.9
IC4964	67	2.394	230	-12 +7	203	-5 +5	12.53	0.03	3028	1.14	1.20	0.32	Pavo	32.32	0.22	10.6	8.5
IC4992	90	2.477	304	-9 +9	284	-8 +8	12.31	0.03	4068	1.20	1.35*	0.87	Pavo	33.10	0.15	7.5	8.0
IC5023	75	2.529	329	-9 +26	301	-12 +11	11.16	0.03	3077	1.05	1.14*	0.43	Pavo	32.52	0.23	9.1	6.9
IC5060	77	2.178	149	-14 +17	126	-11 +10	13.38	0.12	4127	0.82	0.93	0.48	HSB	30.05	**	5.9	1.8
IC5071	90	2.592	395	-5 +4	370	-5 +5	10.07	0.03	2995	1.42	1.56	0.68	Pavo	32.09	0.06	16.5	25.0
73-4	60	2.645	385	-19 +11	355	-11 +14			3546	0.99	1.03*	0.24	NoPhot	***	**	5.9	7.9
74-4	79	2.293	195	-20 +5	160	-6 +5	13.83	0.03	3158	0.92	1.03*	0.51	Pavo	32.24	0.43	8.5	6.9

TABLE 3

NONDETECTIONS

CLUSTER	Galaxies Not Detected
Antlia	317-6, 376-23, IC 2578, NGC 3258, NGC 3258E, NGC 3281
NGC 3557	318-22, 318-29, 377-10
Hydra	437-25, 437-31, 437-47, 500-31, 501-8, 501-11, 501-42, 501-69, 501-75, 501-80, 501-81, 501-90, 501-98
Centaurus	269-49, 322-33, 322-93, 323-2, 323-6, 323-46, 323-98, 325-25, NGC 4696A, NGC 5011A
ESO 508	509-19, 509-23, 576-12, 576-26, 576-31, IC 4231
Pavo	47-22, 73-7, 73-12, 73-14, 106-9, IC 4929, IC 4945, IC 4903, NGC 6808
Telescopium[a]	233-31, 233-36, 235-53, 235-75, 236-6, 284-2, 284-20, 286-16, 286-18, 286-36, 286-76, NGC 6861E, NGC 6870

[a] Two detections were in fact obtained in this cluster: NGC 6861F and NGC 6875A. These will be discussed elsewhere.

TABLE 4

COMPARISON OF 21 CENTIMETER PARAMETERS

Galaxy	v^a km s^{-1}	v^* km s^{-1}	ΔV_{20} km s^{-1}	$\Delta V_{20}{}^*$ km s^{-1}	F_{HI} Jy km s^{-1}	$F_{HI}{}^*$ Jy km s^{-1}	Reference*
NGC 4603	2608	2562	411 ± 14	495 ± 60	22.7	36.2 ± 8.0	1
IC 2531	2470	2477	535 ± 34	491 ± 15	40.3	53.4 ± 33.	1
NGC 3223	2912	2900	411 ± 10	425 ± 25	22.0	30.0 ± 7.0	1
508-11	2606	2606	264 ± 7	270	21.8	24.0 ± 2.5	2
NGC 3285	3430	3378	575 ± 30	594	6.9	9.79 ± 3.9	2
437-4	3326	3299	330 ± 12	329	6.8	7.9 ± 0.9	2
501-68	3109	3095	351 ± 29	333	3.3	3.8 ± 0.52	2
501-1	3829	3776	267 ± 6	264	18.1	19.1 ± 2.2	2
507-67	3069	3089	205 ± 8	337	7.1	14.7 ± 1.8	2
443-79	2129	2220	148 ± 8	165	10.8	8.2 ± 0.97	2
576-11	2776	2735	331 ± 16	354	16.1	24.8 ± 2.9	2
NGC 3568	2425	2444	307	343	32.2	29.8 ± 10	2
IC 4237	2672	2643	309 ± 12	317	12.4	11.9 ± 1.4	2
NGC 7591	4954	4952	410 ± 20	436 ± 17			3
NGC 7610	3549	3551	287 ± 13	282 ± 6			3
NGC 7750	2942	2944	251 ± 6	252 ± 20			3
NGC 7757	2954	2959	183 ± 7	175 ± 4			3
U12423	4851	4850	521 ± 9	535 ± 14			3

REFERENCE.—(1) Fisher and Tully 1981; (2) Richter and Huchtmeier 1987; (3) Bothun *et al.* 1985.

[a] Heliocentric velocity.

TABLE 5

APERTURE PHOTOMETRY

Obj	Ap	H	Obj	Ap	H	Obj	Ap	H	Obj	Ap	H	Obj	Ap	H
N3223	59.2	8.80	437-56	32.0	11.13	377-31	32.0	11.59	N4672	31.6	10.52	576-32	32.0	10.98
LC40	69.5	8.65				LC40	42.0	11.19	LC40	46.7	10.24	LC40	42.0	10.90
LC40	46.7	9.04	N3285	42.0	9.44									
LC40	42.0	9.15	LC40	53.0	9.19	N3573	59.2	9.33	323-27	31.6	10.84	507-41	21.1	12.69
LC40	53.0	8.92	CT60	38.1	9.37	LC40	69.5	9.22	LC40	46.7	10.46	C100	28.0	12.35
			CT60	48.6	9.26				C100	32.1	10.88:			
N3347A	31.6	10.69				378-11	21.1	12.35				508-11	28.0	12.50
LC40	46.7	10.30	501-1	32.1	12.47	C100	28.0	12.14	322-42	20.7	12.43	LC40	42.0	11.83:
C100	20.7	11.25:	LC40	42.0	12.10	C100	20.7	12.35	C100	32.1	12.00	LC40	21.1	12.96
C100	32.1	10.74:				C100	32.1	12.05	LC40	32.0	11.90			
LC40	59.2	10.11	501-2	20.7	11.85				LC40	42.0	11.58:	443-79	20.7	14.04
			LC40	32.1	11.58	377-40	21.1	14.11	C100	32.1	12.11	C100	32.1	13.57
N3347B	46.7	11.12				C100	28.0	13.99						
CT60	59.2	10.78	437-4	32.0	11.11				268-37	21.1	12.09	507-42	21.1	11.44
			LC40	42.0	10.72	N3533	46.7	9.94	C100	28.0	11.87	C100	28.0	11.30
318-4	31.6	10.76				LC40	59.2	9.82						
LC40	46.7	10.29	437-30	42.0	10.13	LC40	69.5	9.73	323-73	21.1	11.67	508-7	32.1	12.94
C100	20.7	11.06	LC40	53.0	10.00				C100	28.0	11.46			
C100	32.1	10.61	CT60	38.1	10.28	268-46	32.1	12.43	C100	20.7	11.66	576-40	21.1	12.71
			CT60	48.6	10.08	CT60	38.1	12.87	C100	32.1	11.39	C100	32.1	12.34
I2531	59.2	9.57				CT60	48.6	12.56				C100	28.0	12.48
LC40	69.5	9.49	501-86	20.7	11.98				322-48	21.1	12.50			
LC40	53.0	9.95:	C100	32.1	11.53	321-25	31.6	11.22	C100	28.0	12.23	I4992	21.1	12.72
LC40	64.0	9.61:	CT60	38.1	11.37	LC40	46.7	10.85	C100	20.7	12.40:	C100	28.0	12.43
			CT60	48.6	11.06	LC40	59.2	10.51						
N3449	46.7	9.34							323-39	20.7	13.22	I5060	13.6	13.38
LC40	59.2	9.22	501-68	32.1	11.45	268-44	21.1	11.47	C100	32.1	12.96	LC40	21.1	13.17
LC40	42.0	9.38	CT60	38.1	11.32	C100	28.0	11.26	LC40	21.1	13.30	LC40	11.0	13.39
LC40	53.0	9.24	CT60	48.6	11.11	C100	20.7	11.30	C100	28.0	13.07	CT60	22.1	13.07
LC40	46.7	9.27	LC40	32.0	11.50	C100	32.1	11.09						
									N4679	31.6	10.35	I4934	21.1	12.69
I2556	21.1	12.97	501-82	32.1	11.02	269-28	21.1	13.00	LC40	42.0	10.24	C100	28.0	12.27
C100	28.0	12.56	LC40	32.0	11.08	C100	28.0	12.71	LC40	46.7	10.11			
			CT60	38.1	11.00				LC40	59.2	9.98	I4962	13.6	14.96
I2559	32.0	11.11	CT60	48.6	10.85	269-52	21.1	13.78	LC40	53.0	10.15:	LC40	21.1	14.49
C100	32.1	11.16				C100	28.0	13.60						
			319-11	38.1	11.35				323-25	31.6	10.50	I5023	21.1	11.19
I2560	42.0	9.75	CT60	48.6	11.13	322-85	21.1	12.98	LC40	46.7	10.21	C100	28.0	10.91
LC40	53.0	9.55	C100	20.7	11.63	C100	28.0	12.63						
LC40	46.7	9.71	C100	32.1	11.33				507-67	42.0	11.37	74-4	13.6	14.01
LC40	59.2	9.53	LC40	42.0	10.97:	323-72	21.1	12.51	LC40	53.0	11.15	LC40	21.1	13.57
LC40	69.5	9.40				C100	28.0	12.29						
			N3568	31.6	10.43				508-19	20.7	12.59	I4964	21.1	12.78
437-14	31.6	10.08	LC40	46.7	10.08	381-14	21.1	13.01	C100	32.1	12.08	C100	28.0	12.49
LC40	46.7	9.87	LC40	59.2	9.91	C100	28.0	12.69	LC40	32.0	12.08:			
LC40	42.0	9.94				C100	20.7	12.94				N6943	55.8	9.42
LC40	53.0	9.83	377-34	32.0	11.87	C100	32.1	12.65	576-11	32.0	11.45	CT60	70.1	9.17
CT60	38.1	10.02	LC40	42.0	11.58				LC40	42.0	10.93	LC40	42.0	9.80
CT60	48.6	9.85	CT60	38.1	11.88	N4575	20.7	10.92				LC40	53.0	9.54
						C100	32.1	10.46	N5022	32.0	10.30			
N3463	20.7	10.96	378-3	31.6	11.58				LC40	42.0	10.06	I5071	42.0	10.30
C100	32.1	10.68	LC40	46.7	11.10	N4603A	20.7	10.96	C100	32.1	10.30	CT60	55.8	9.97
			LC40	42.0	11.32	C100	32.1	10.73				CT60	70.1	9.80
437-34	20.7	13.51	LC40	53.0	11.05	LC40	31.6	10.76	IC4237	42.0	10.31			
						LC40	46.7	10.56	LC40	53.0	9.86	N7083	55.8	9.23
437-54	20.7	12.24	377-21	31.6	11.45							CT60	70.1	8.98
C100	28.0	12.02	LC40	46.7	11.14	N4603	59.2	9.60	508-51	21.1	13.43	LC40	42.0	9.54
C100	32.1	11.95	C100	32.1	11.53:	LC40	69.5	9.33	C100	32.1	12.84	LC40	53.0	9.28
									C100	28.0	13.01			

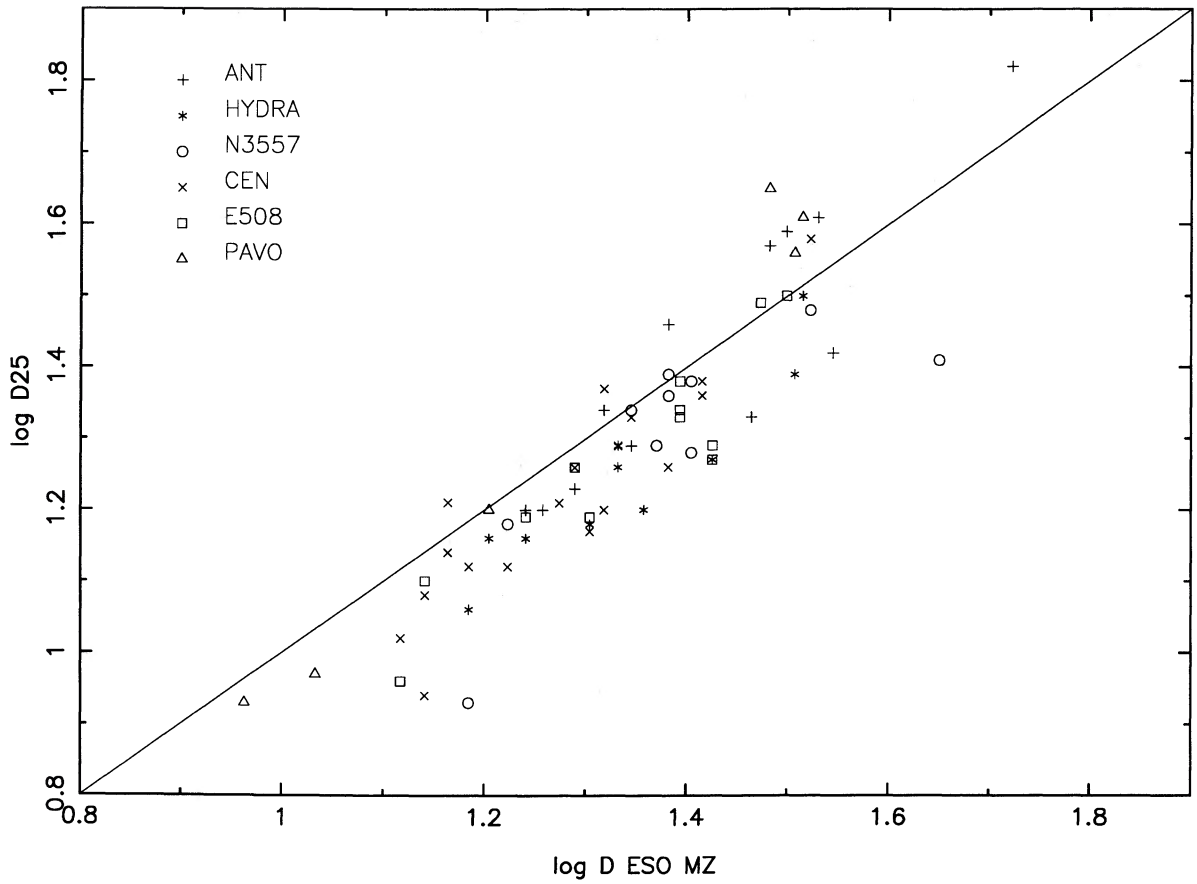

FIG. 2.—A comparison of measured isophotal major diameters with estimates of that quantity from the ESO atlas of Lauberts (1982), transformed according to Mould and Ziebell (1982). Values of D_{25} are expressed in tenths of arcminutes. The symbol key for different clusters is shown.

growth curve slope seen in the sample, in the few cases where aperture extrapolation was required.

V. TULLY-FISHER RELATIONS AND CLUSTER DISTANCES

To locate the galaxies in the Tully-Fisher diagram the inclination of the plane of the disk to the plane of the sky was calculated in the standard way (Aaronson, Mould, and Huchra 1980), and is given in column (2) of Table 2. The 20% velocity width was then corrected to the edge-on value $\Delta V(0)$ (col. [3]) and used to construct Figure 3*a* for the six clusters observed. Following Lucey, Currie, and Dickens (1986*a*) we have separated the Centaurus cluster at 4150 km s^{-1} heliocentric into two subclusters, Cen 30 and Cen 45. The Tully-Fisher diagram for the small Cen 45 sample is shown in Figure 3*b*.

Examining Figure 3 cluster by cluster, we begin with Antlia, which shows a very tight correlation of luminosity and velocity width. The galaxy plotted as an open circle in Antlia is IC 2531 which falls outside the 4° radius specified in Table 1. This is signified by the "Out" flag in column (16) of Table 2. If we fit the calibration relation adopted by Aaronson *et al.* (1986) (eq. [4]), we obtain distance moduli for the individual galaxies in Antlia. These are recorded in column (17) of Table 2, together with the uncertainty in modulus (col. [18]) resulting from the velocity width and magnitude uncertainties. The values in

TABLE 6

MEAN PROPERTIES OF THE CLUSTER SAMPLE

Cluster (1)	Cluster $\langle v_0 \rangle$ (km s^{-1}) (2)	Sample $\langle v_0 \rangle$ (km s^{-1}) (3)	σ_v (km s^{-1}) (4)	n (5)	$\langle m-M \rangle$ (mag) (6)	σ_{m-M} (mag) (7)	Cluster $\langle r \rangle$ (Mpc) (8)	$\langle \Delta\Sigma \rangle$ (mag) (9)
Antlia	2667 ± 84	2662	203	10	32.34	0.30	29 ± 1	0.15 ± 0.21
Hydra	3455 ± 85	3444	390	10	33.18	0.49	43 ± 3	0.11 ± 0.15
NGC 3557	2702 ± 79	2753	129	5	32.67	0.33	34 ± 2	−0.08 ± 0.14
Cen 30	2804 ± 52	3157	542	10	32.44	0.59	31 ± 3	−0.12 ± 0.16
Cen 45	4337 ± 35	4478	313	6	33.33	0.56	46 ± 5	0.10 ± 0.16
ESO 508	2728 ± 60	2692	166	7	32.24	0.54	28 ± 3	−0.49 ± 0.14
Pavo	3651 ± 123	3229	332	8	32.48	0.37	31 ± 2	−0.11 ± 0.18

NOTES.—Velocity v_0 is relative to the Local Group centroid. $\Delta\Sigma = \Sigma^{\rm Obs} - \Sigma^{\rm Pred}$, where the prediction is from the fiducial line in Fig. 5.

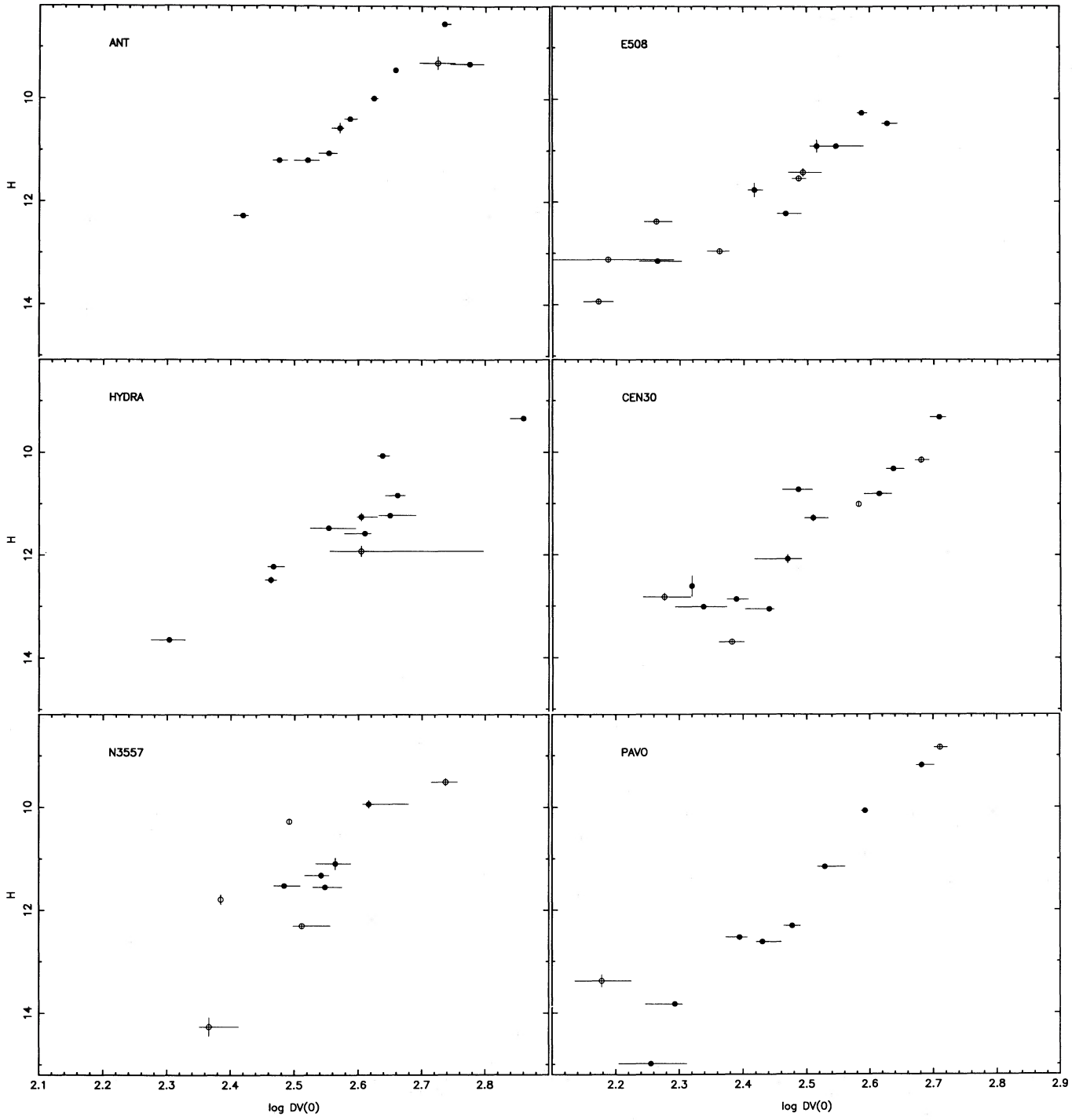

FIG. 3*a*

FIG. 3*a*—Tully-Fisher diagrams for six clusters of the Parkes sample. Values of $H = H^{c}_{-0.5}$ are from col. (10) of Table 2. Values of log $\Delta V(0)$ are in col. (3). Open circles denote galaxies which have been excluded from the cluster samples for reasons coded in col. (16) and explained in the text. (*b*) Tully-Fisher diagram of the Cen 45 Cluster.

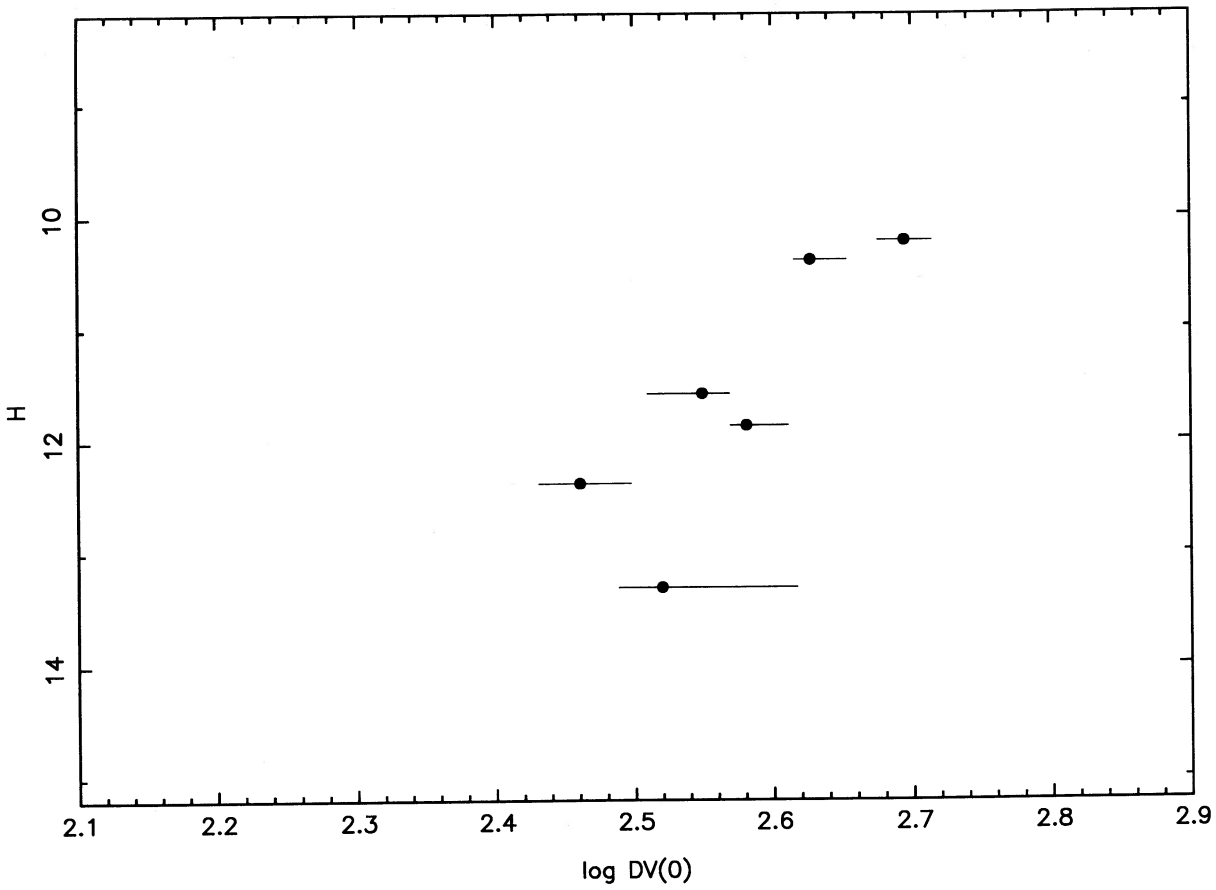

FIG. 3*b*

column (18) are dominated by the velocity width uncertainty, but are still much less than the 0.45 mag scatter generally seen in the IRTF relation (Aaronson and Mould 1983). Over the sample as a whole the scatter in Figure 3 is apparently intrinsic to this formulation of the Tully-Fisher relation, and exceeds what can be explained by observational error. Accordingly, in computing the mean distance modulus given in Table 6, we have weighted only the individual galaxy moduli by the observational error if the value in column (18) exceeds 0.45 mag.

In the Hydra cluster the galaxy 501-2 has a nominal ΔV_{20} of 608 km s^{-1}, clearly affected by noise in the profile. This value was replaced in Table 2 by 1.1 times ΔV_{50}. The asterisks in column (18) indicate the galaxy was rejected from the cluster modulus mean. This galaxy is flagged "Low SN" in column (16).

Examination of the velocity histogram for the NGC 3557 group shows a more complicated structure in redshift space than the preceding clusters. Within the velocity range isolated in Table 1 there is a low-dispersion (σ = 125 km s^{-1}) group centered on the prototype elliptical galaxy, and foreground and background groups 2 σ away from this. These latter galaxies are identified "Fore" and "Back" in column (16) of Table 2 and are rejected from the sample mean. The correlation between distance and redshift in this sample is shown in Figure 4*a*. The line drawn through these data is: $v = \langle v/r \rangle r$ where r is the ordinate and v the abscissa. A previous example of a "cluster" like this, in which subgroups have not separated from the Hubble flow, is the Cancer Cluster (Aaronson *et al.* 1986).

The Centaurus Cluster also has complex structure in redshift space, and this has been explored in depth by Lucey, Currie, and Dickens (1986*b*). Again a correlation is seen between distance and redshift. Open circles in Figure 4*b* refer to NGC 4575, which does not satisfy the inclination criterion ($i > 45°$) of Aaronson, Mould, and Huchra (1980), and 323−72, which is rejected from the sample as a "high surface brightness" outlier (see § VI). This galaxy's confused 21 cm profile was remarked on in § II. These two galaxies and also 321−25 and 269−52 are denoted by open circles in Figure 3. The latter two galaxies lie outside a 4° cluster defining radius. As indicated by the asterisks in Table 2, all four galaxies are excluded from the cluster distance and redshift means compiled in Table 6.

Only seven Cen 45 galaxies were observed, and (excluding the face-on galaxy 322−76) these are shown in Figure 3*b*. In Table 6 we see a 3 σ separation between mean distances of the two clusters. This difference would remain statistically significant, if the most distant galaxy 323−39 were excluded. This contradicts an earlier claim (Aaronson *et al.* 1987) of "no clear separation." Discovery of a systematic photometric error affecting some Centaurus and most Pavo galaxies is the cause of this revision. The Centaurus sample has also been enlarged from 12 to 20 galaxies since 1987. Figure 4*b* does not help us to understand the distribution of galaxies in coordinate space compared with the bimodal distribution in redshift space. We shall treat Centaurus as two clusters, although the real situation may be more complex.

The ESO 508 sample is affected by the presence of a foreground group in the heliocentric velocity range 1300 to 2400

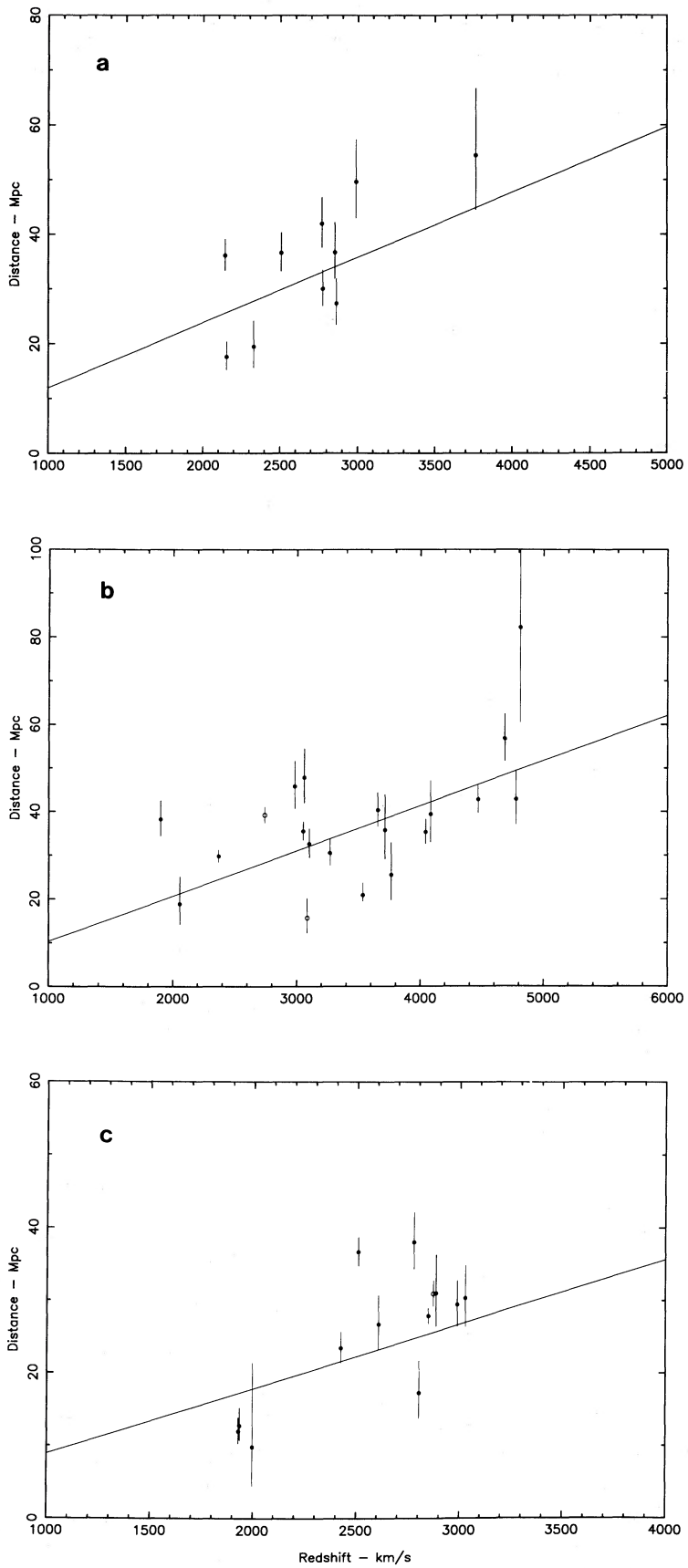

FIG. 4*a* (*top*).—The correlation between distance and redshift for the NGC 3557 group. The line represents the relation $v = \langle v/r \rangle r$ for this unvirialized group. Velocities are in the rest frame of the Local Group. (*b*) (*center*) The correlation between distance and redshift for the Centaurus Cluster(s). The open circles denote the too close to face-on galaxy NGC 4575 and the problem galaxy 323 – 72. (*c*) (*bottom*) The correlation between distance and redshift for the ESO 508 group. There seems to be two subgroups. The open circle denotes the low-inclination galaxy 507 – 67.

km s^{-1}. Three of our sample belong in this foreground group based on their velocities, and are so signified in Table 2 and Figure 3. One of these galaxies, 508−51, was detected at the edge of the correlator bandpass. The value of ΔV_{20} in Table 2 is 1.1 times ΔV_{50} for this object. We also observed two galaxies which lie outside a 4° inclusion radius and one low-inclination galaxy, which are also denoted as open circles in Figure 3. The original sample of 13 galaxies is down to seven in Table 6. The reality of the foreground group is clearly seen in the distance-redshift correlation of Figure 4*c*.

Finally there is the Pavo Cluster, located on the opposite (south) side of the Galactic plane from the other five clusters. A good correlation between luminosity and velocity width is seen, spanning 6 mag. Three galaxies were excluded from the Table 6 cluster mean on the basis of high surface brightness, angular distance from the cluster center, or lack of photometry. Disagreement at the 2.5 σ level between the cluster mean velocity and the sample mean velocity suggests once again a complex structure for this cluster.

The results are summarized in Table 6. The mean velocity of the cluster $\langle v_0 \rangle$ and its uncertainty are given in column (2). The mean velocity of the sample, its dispersion in velocity, and the number of members are contained in columns (3), (4), and (5). Columns (6) and (7) give the mean distance modulus $\langle m-M \rangle$ of the sample and the sample dispersion in modulus. The cluster distance $\langle r \rangle$ corresponds to $\langle m-M \rangle$ and is noted in column (8).

VI. SURFACE BRIGHTNESS SYSTEMATICS

Because surface brightness has proved to be an important member of the manifold of elliptical galaxy structural parameters, it may be useful to consider the distance-independent quantity, $\Sigma_H = H^c_{-0.5} + 5 \log D_1$. Aaronson *et al.* (1986) compared the correlation between surface brightness and line width for the clusters of the Arecibo sample and found an apparently systematic behavior with redshift. Figure 5 shows the correlation for the Parkes sample together with the fiducial mean line for the Virgo and Ursa Major Clusters. The net deviation from this line is noted in Table 6, and is only significant in the case of the ESO 508 group. Curiously, five of the six high surface brightness galaxies in this group have been rejected from the cluster sample on other grounds. The two galaxies which are more than 3 σ deviant from fiducial line are 323−72 in Centaurus and IC 5060 in Pavo. As indicated in the previous section, these have been rejected from the cluster samples.

Figure 5, being comprised of distance-independent quantities, may serve to constrain the effects of cluster dynamical evolution on disk galaxies. If such evolution is responsible for falling rotation curves in cluster galaxies (Whitmore, Forbes, and Rubin 1988), or stripping of outer parts of galaxies, we would expect to see the affected galaxies fall systematically below the mean relation in Figure 5. However, setting aside ESO 508, we see no correlation between $\Delta\Sigma$ in column (9) of

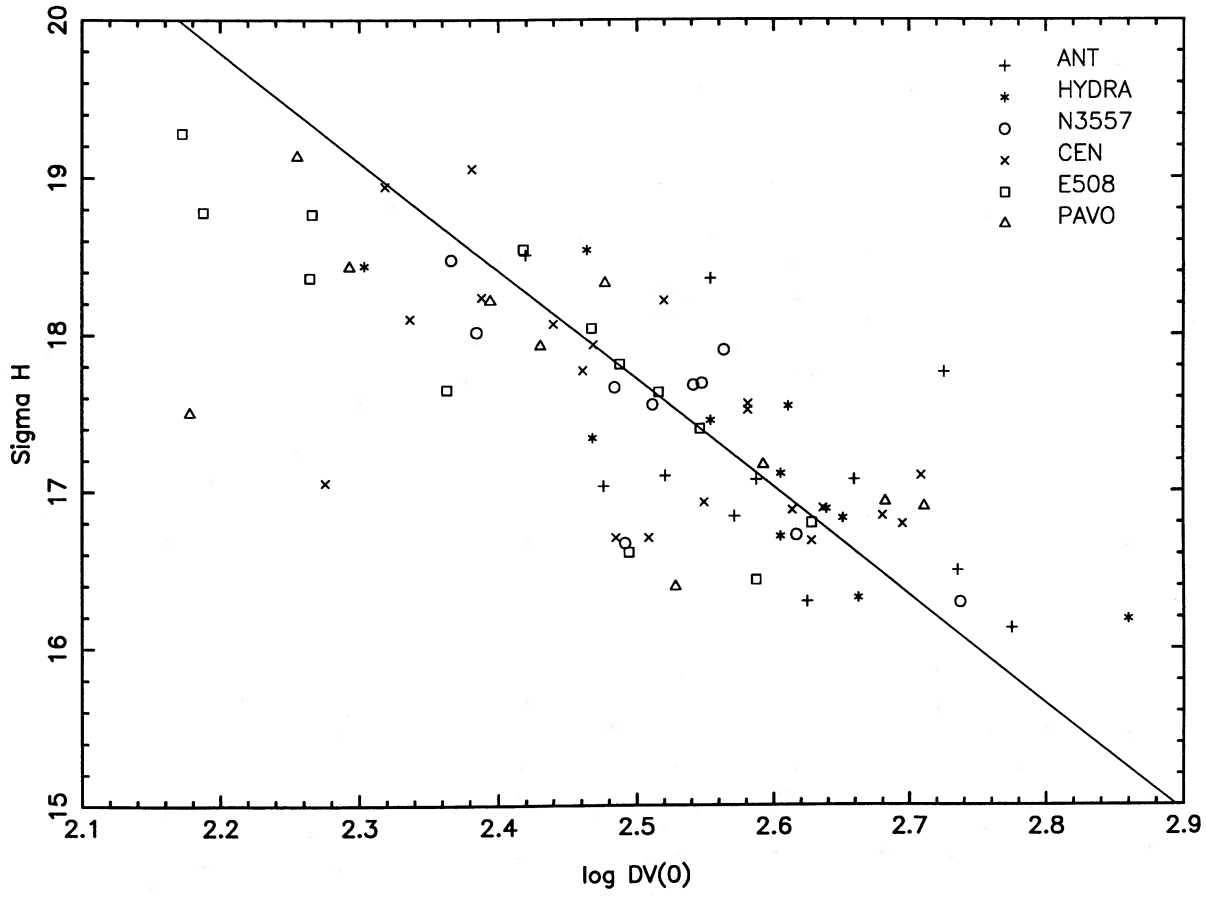

FIG. 5.—The correlation between H surface brightness Σ_H and velocity width. The fiducial line is a fit to the relation populated by galaxies in the Virgo and Ursa Major Clusters (Aaronson *et al.* 1986).

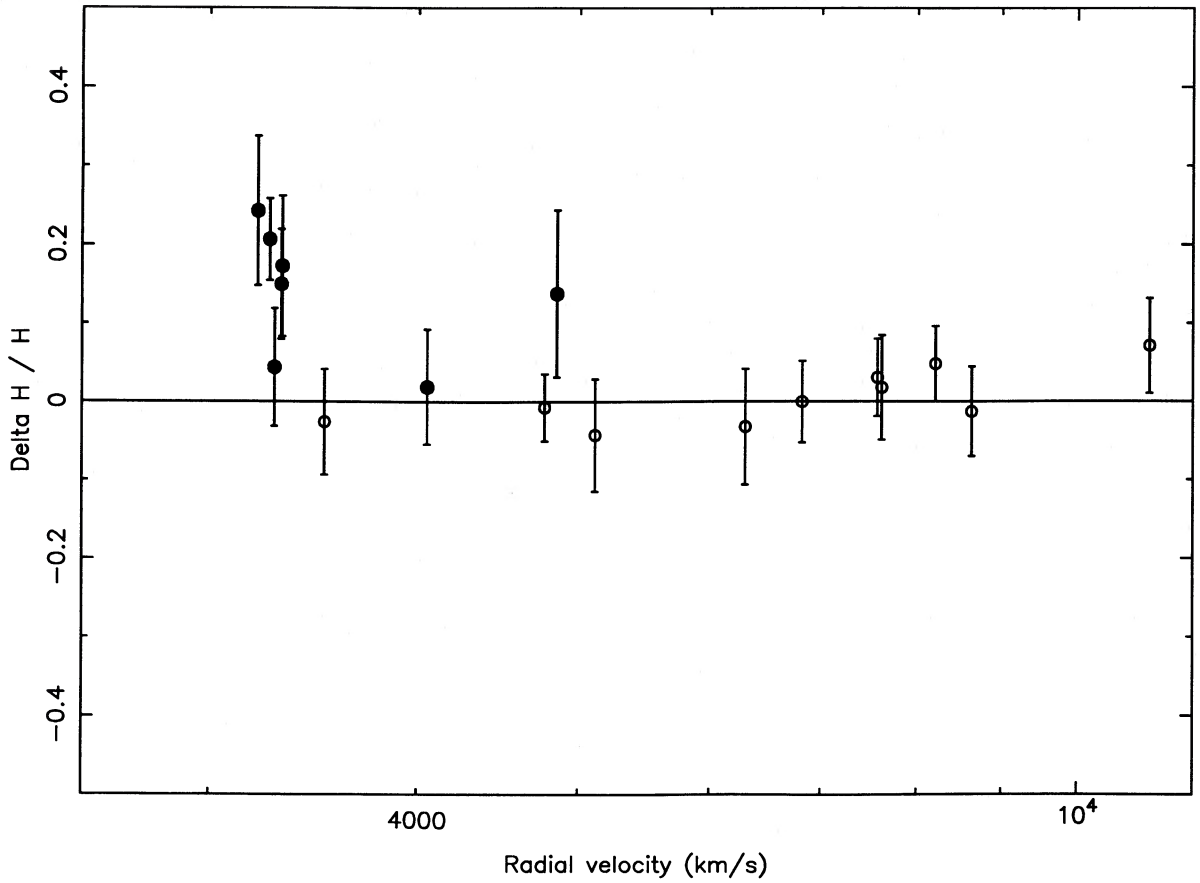

FIG. 6.—Deviations from uniform Hubble flow $\Delta H/H_0$ plotted against cluster redshift. The Arecibo clusters (*open symbols*) define H_0 asymptotically. Five of the seven Parkes clusters deviate from this value by more than 1 σ. The radial velocity in the CMB frame is plotted logarithmically with 1000 km s^{-1} tick marks.

Table 6 and the peculiar velocities inferred in the next section. In the Arecibo sample (Aaronson *et al.* 1986) it is possible to show (but beyond the scope of the present paper) that the correlation of $\Delta\Sigma$ with redshift is reduced, if the straight line fit to Virgo and Ursa Major in Figure 5 is replaced by a quadratic. Selection in favor of large ΔV galaxies in more distant Arecibo clusters seems to be responsible for the large systematic residuals noted by Aaronson *et al.* Further investigation is required of any remaining residuals and their correlation with other variables.

VII. DEVIATION FROM A UNIFORM HUBBLE FLOW

If the Local Group is moving with a velocity of 600 km s^{-1} in the direction $l = 268°$, $b = 27°$, as has been inferred from the dipole anisotropy in the microwave background radiation (Lubin, Epstein and Smoot 1983; Fixsen, Cheng, and Wilkinson 1983), the kinematics of the cluster sample will assume their simplest form when transformed to a frame which has been corrected for this motion of the observer. Aaronson *et al.* (1986) found the motions of their Arecibo cluster sample to be random with v_{rms}(pec) less than 500 km s^{-1} after this transformation to the cosmic microwave background (CMB) frame. This can be seen in the distribution of open symbols representing the Arecibo clusters in Figure 6. The ordinate of Figure 6, $\Delta H/H_0$, is calculated from the transformed cluster velocity and cluster distance in Table 7, using the asymptotic value of $H_0 =$ 92 km s^{-1} Mpc^{-1}, obtained from the Arecibo clusters by Aaronson *et al.* (1986). This value of H_0, of course, depends on

TABLE 7

PECULIAR VELOCITIES AND HUBBLE RATIOS

Cluster	$\langle v\rangle$[a]	$\langle m-M\rangle$	±	v_{pec}	±	$\langle v\rangle/\langle r\rangle$	$\langle v/r\rangle$
Antlia	3261	32.34	0.09	559	140	111.0 ± 5.8	109.7 ± 4.7
Hydra	4055	33.18	0.15	76	288	93.8 ± 6.9	95.8 ± 7.5
NGC 3557	3284	32.67	0.15	138	231	96.0 ± 7.2	102.7 ± 9.3
Cen 30	3314	32.44	0.19	489	253	107.9 ± 9.6	112.7 ± 10.4
Cen 45	4847	33.33	0.23	588	453	104.7 ± 11.1	109.3 ± 8.3
ESO 508	3215	32.24	0.20	627	245	114.3 ± 10.8	134.5 ± 12.7
Pavo	3314[b]	32.48	0.13	432	208	105.8 ± 7.4	108.5 ± 4.3

[a] Velocity relative to the cosmic microwave background frame.
[b] This is the sample mean velocity from Table 6, not the cluster mean.

the zero point of the calibration of the IRTF adopted by Aaronson *et al.* But Figure 6 has no such dependence, as is clear from the dimensionless character of the ordinate. All that is required is that an asymptotic value of H_0 should exist at redshifts very much greater than any local peculiar velocities.

Five out of seven of the clusters in the present sample, however, show positive values of $\Delta H/H_0$ with a significance greater than 1 σ. If one calculates $\langle v/r \rangle$ for each cluster rather than $\langle v \rangle / \langle r \rangle$, generally similar results within the uncertainties are obtained. This comparison can be made in the right-hand columns of Table 7. In the case of the ESO 508 group, the foreground group is the source of the difference between $\langle v/r \rangle$ and $\langle v \rangle / \langle r \rangle$. Figure 6 suggests that some elements of the Hydra-Centaurus Supercluster deviate significantly (i.e., by more than 2 σ) from the uniform Hubble expansion that characterizes the kinematics of the clusters of galaxies we have studied up to now. The peculiar velocities of the sample in the CMB frame are given in Table 7, calculated as follows: $v_{pec} = \langle v \rangle - 92\langle r \rangle$. Again it should be emphasized these values are independent of $H_0 = 92$ km s^{-1} Mpc^{-1}. If one multiplies the distances to the IRTF calibrating galaxies by 2, then $\langle r \rangle$ is doubled and $H_0 = 46$ km s^{-1} Mpc^{-1}. The values of v_{pec} remain the same.

It is possible to compare our inferred peculiar velocities with those obtained for elliptical galaxies in the same clusters. But first we shall examine whether the cluster distances as a whole are consistent. When subjected to the criteria in Table 1, the sample of Davies *et al.* (1987) and Burstein *et al.* (1987) offer four galaxies in the Antlia Cluster for comparison, one in ESO 508, three in NGC 3557, one in Pavo, three in Hydra, eight in Cen 30, and four in Cen 45. If we form the quantity $x = D_{galaxy}/(92\langle r \rangle)$, where D_{galaxy} is calculated from equation (1) of Dressler *et al.* (1987) and $\langle r \rangle$ is given in Table 6, we obtain $\langle x \rangle = 0.94 \pm 0.07$ by lumping all the clusters together.[14]

Our peculiar velocity for Hydra of 76 ± 288 km s^{-1} is consistent with -168 ± 511 (Faber *et al.* 1988) and -203 ± 255 found by Lucey and Carter (1988). However, for Antlia our highly significant result of 559 ± 140 km s^{-1} disagrees with $v_{pec} = -174 \pm 299$ km s^{-1} obtained by Faber *et al.* Our result for Cen 30 of 489 ± 253 km s^{-1} is smaller than the peculiar velocity indicated by Faber *et al.* (1988) of 1110 ± 208 km s^{-1}, and does not disagree with that obtained by Lucey and Carter, 224 ± 277 km s^{-1}. Finally, for Cen 45 large uncertainties preclude any useful comparison: we obtain $v_{pec} = 588 \pm 453$ km s^{-1}; Faber *et al.* find 1663 ± 334; but Lucey and Carter measure 2193 ± 436 km s^{-1}. Lucey *et al.* (1986*b*) have suggested that a background system contributes to Cen 45. If the spirals observed here are drawn from this background, and the ellipticals form a separate group, these highly discrepant results could be understood. Further work on Cen 45 is clearly needed. Substructure could possibly be invoked in the case of Antlia too.

We draw two conclusions from the comparison of the spiral and elliptical data. First there is no clear evidence of a systematic difference between Parkes data distances and Faber *et al.* (1988) distances to clusters in common. Second, on a cluster-by-cluster basis there are significant discrepancies between the peculiar velocities of the spiral and elliptical samples, which may be a result of substructure. This will probably only be resolved by a much fuller mapping of the Hydra-Centaurus Supercluster. Therefore, while every care has been taken to avoid systematic effects between our northern and southern hemisphere work, their absence below the 7% (1 σ) level cannot be verified in this way without further study of less confused clusters. A hypothetical systematic uncertainty in $\Delta H/H_0$ at this level has not been included in the purely random error bars displayed in Figure 6.

[14] An alternative comparison is based on Table 4 of Faber *et al.* (1988) and distance moduli from Table 8 of the present paper. For seven Parkes clusters in common (ESO 508 is not in common; we have added Fornax) the ratio Faber/IRTF is 1.01 ± 0.07. For five Arecibo clusters (Pisces, A1367, Coma, Pegasus, and Virgo) the ratio is 1.02 ± 0.02.

VIII. A KINEMATIC MODEL: THE VIRGO-HYDRA-CENTAURUS SUPERCLUSTER

Most of the clusters in the combined Parkes and Arecibo samples, whose properties are summarized in Table 8, lie close to the supergalactic plane. This flattening may in itself be a clue that we should look to larger scales in order to understand significant peculiar velocities. Figure 7 is a polar diagram of the distribution of clusters. They are plotted on the supergalactic plane at their measured radii from the Local Group. The plotted azimuth is supergalactic longitude. This plane is the optimum representation; the apparent relative positions of the clusters closely approximate the true ones. With the exclusion of the Cancer Cluster at supergalactic latitude $-48°$, the dispersion of the clusters about the supergalactic plane is 18°. Figure 7 also shows the observed component of their peculiar velocities. The filled symbols are plotted at radius vector 92 $\langle r \rangle$ km s^{-1} and the "tails" point to $\langle v \rangle$ km s^{-1}, indicating the size of the measured v_{pec}. Open symbols indicate the location of clusters in the samples[15] of Geller and Huchra (1982) from the (northern) CfA survey and of Sandage (1975) from his southern redshift survey. These clusters are plotted supposing that their unmeasured peculiar velocities are zero.

The size of the cluster is indicated by the radius of the circle via the following scheme Galaxies in Virgo larger than 6′ in the UGC (Nilson 1973) were counted in a 15° box. Galaxies were counted in other clusters with scaled angular dimensions in the UGC and ESO catalogs. The completeness limits of these catalogs should make this fairly unbiased representation of the local 8000 km s^{-1} radius region, with the proviso that some clusters (as opposed to galaxies in clusters) will have been missed due to the limitations of the cluster catalogs. Indeed, the Perseus Cluster centered on NGC 1275 had to be added by hand. The largest redshift in Sandage's work is 4900 km s^{-1}, his survey being confined to Shapley-Ames galaxies.

Figure 7 suggests that the volume containing the Local Supercluster and the Hydra-Centaurus Supercluster shares a common peculiar velocity of order 300 km s^{-1} in the direction of supergalactic longitude 135°. Indeed, Tully and Fisher (1987) regard the Virgo-Hydra-Centaurus Supercluster as a single entity in a structural map on 50 Mpc scales. And this view was also the first impression of Dressler *et al.* (1987) of the kinematics of elliptical galaxies within this volume. The volume they considered to partake in this bulk flow was larger than is apparent in Figure 7, and the bulk peculiar velocity was larger too. But the notion of a bulk flow of Virgo-Hydra-Centaurus is a good summary of what is seen in Figure 7. If Virgo-Hydra-Centaurus is taken to include Virgo, Ursa Major, Hydra, Antlia, Centaurus, NGC 3557, and ESO 508, and if we assume the bulk flow is in the direction of the microwave

[15] From Sandage (1975) Figure 7 shows the NGC 4373, 4936, 6769, and 7196 groups, the IC 4296, 4329, and 4797 groups, and the Telescopium and Indus Clusters. From Geller and Huchra (1982) Figure 7 shows HG 6, 30, 73, 92, 101, 119, 141 and 173.

TABLE 8

THE ARECIBO AND PARKES SAMPLES[a]

Cluster	l	b	$\langle v_0 \rangle$	σ_v	$\langle m-M \rangle$	$\sigma_{\langle m-M \rangle}$
Pisces	125.8	−32.5	5274	58	33.59	0.09
A400[b]	170.3	−44.9	7855	135	34.55	0.14
A539	195.7	−17.7	8561	123	34.89	0.12
Cancer	202.5	28.7	4790	89	33.82	0.15
A1367	234.8	73.0	6427	73	34.35	0.11
Coma[b]	57.2	87.9	7310	132	34.51	0.10
Z74-23	349.6	65.5	6025	153	34.25	0.15
Hercules	31.7	44.5	11077	97	35.25	0.13
Pegasus	87.8	−48.4	4078	78	32.97	0.14
A2634/66	103.5	−36.0	8783	115	34.65	0.10
Virgo	283.8	74.5	1073	38	30.82	0.12
Hydra	269.6	26.5	3455	85	33.18	0.15
NGC3557	282.0	22	2702	79	32.67	0.15
Cen 30	302.5	21.5	2804	52	32.44	0.19
Cen 45	302.5	21.5	4337	35	33.33	0.23
Antlia	273.0	20	2667	84	32.34	0.09
ESO 508	309.2	39.2	2728	60	32.24	0.20
Pavo[b]	324.4	−34	3229	117	32.48	0.13
Fornax[c]	236.4	−54.3	1340	42	30.57	0.20
UMa[d]	144.6	65.5	1005	33	30.81	0.09

[a] Velocities relative to the Local Group centroid.
[b] Sample mean velocities rather than cluster mean velocities.
[c] Aaronson *et al.* 1981 recalibrated following Aaronson *et al.* 1986.
[d] Aaronson *et al.* 1979 recalibrated following Aaronson *et al.* 1986.

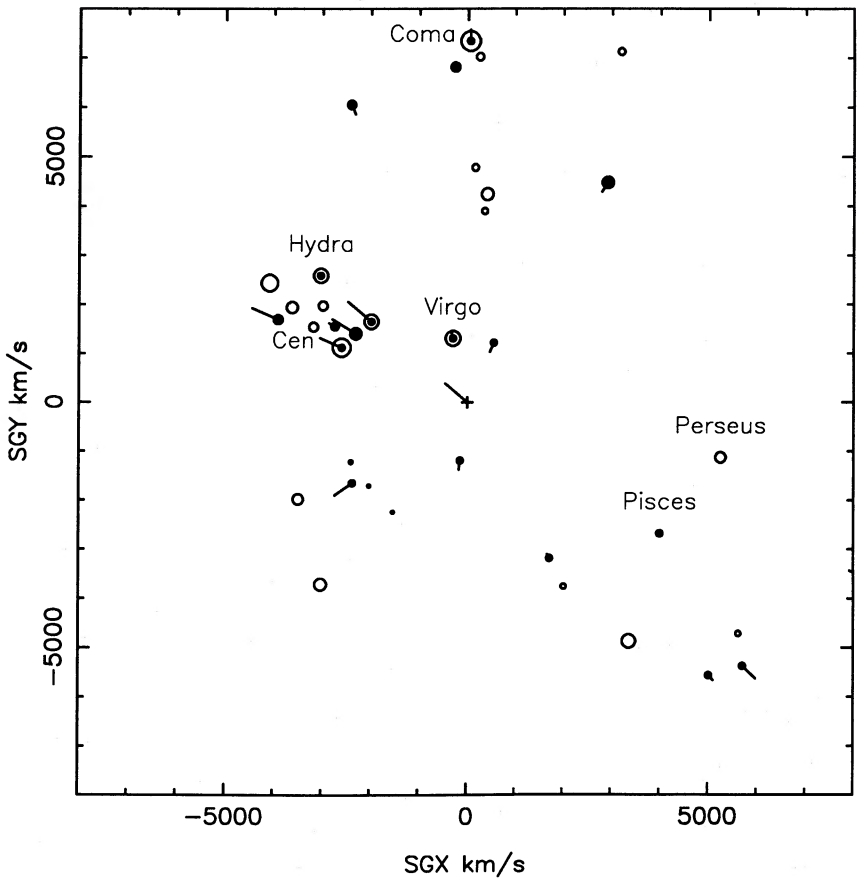

FIG. 7.—Peculiar velocities in the CMB frame for clusters and groups (*solid symbols*) are plotted in polar coordinates. The radius is the IRTF distance of the cluster, and the azimuth is supergalactic longitude. The Local Group is at the origin, and the arrows denoting the size of the peculiar velocity point radially, since that is the only measurable component. Other clusters without measured peculiar velocities and within 8000 km s^{-1} redshift are denoted by open symbols. This is not a volume complete sample, as indicated in the text. The circle size indicates the richness of the cluster. The four major superclusters in this volume are labeled.

background anisotropy, its mean velocity is 275 ± 135 km s^{-1}. For a signal of this strength a simultaneous solution for direction is not possible.

IX. A PARAMETERIZED MODEL: THE "GREAT ATTRACTOR"

Consideration of the origin of such a large-scale flow led Lynden-Bell *et al.* (1988) to propose a model in which a distributed mass concentration is centered at approximately SGX = −4300, SGY = 800 in Figure 7, nicknamed by Dressler (1987) the "Great Attractor." Maps of the galaxy distribution and a redshift survey by Dressler (1988*b*) lend plausibility to the existence of a large concentration of galaxies in this region, possibly extending behind the Galactic plane, which crosses Figure 7 horizontally at SGY = 0.

We shall use a similar, but not identical, model to that described by Lynden-Bell *et al.* That is the "linear bi-infall model" of Han and Mould (1988). That model is a direct extension of the linear Virgocentric flow model of Schechter (1980) to include a second mass concentration at the position of the "Great Attractor." The model is characterized by four free parameters: w_i, the infall velocity at the Local Group position due to the Virgocentric mass distribution, w_j, the local infall velocity due to the "Great Attractor," γ, the power-law index of the radial density fall off of both mass concentrations, and r_{GA}, the distance of the "Great Attractor" center in units of the distance of Virgo. Its direction is taken to be that specified by Lynden-Bell *et al.*

Given the observed velocity of the Virgo Cluster to set the scale in km s^{-1}, this model is capable of predicting the velocity observed in the Local Group centered reference frame at any location in the volume under consideration. The quality of the fit can then be evaluated in terms of χ^2 from the data in Table 8, as follows:

$$\chi^2 = \sum \frac{(v_{\rm pred} - v_{\rm obs})^2}{(\partial v/\partial r)^2 \sigma_r^2 + \sigma_v^2} . \quad (1)$$

The denominator of χ^2 contains the derivative of the predicted velocity (i.e., the local value of the Hubble parameter). The denominator also contains σ_r, the uncertainty in the cluster distance, calculated from $\sigma_{\langle m-M\rangle}$, and σ_v, the uncertainty in the cluster redshift. Automatic χ^2 minimization was used to solve for w_i and w_j. For γ and r_{GA} a map of χ^2 was produced over the parameter space.[16]

In Figure 8 the dashed line separates the plane into two areas: $\chi^2/N > 1.4$ on the right and $\chi^2/N < 1.4$ on the left, where $N = 18$ was taken to be the number of degrees of freedom in the model. A further constraint is needed in order to choose from a wide range of plausible values of distance and concentration. The solid contours in Figure 8 delinate $v_{LG} =$ 550 and 650 km s^{-1}, where v_{LG}, the sum of w_i and w_j, is the resultant velocity of the Local Group. The intersection of this region with $\chi^2/N < 1.4$ is a small region of parameter space: $r_{GA} = 3.35 \pm 0.1$ and $\gamma = 1.8 \pm 0.1$. The corresponding velocity of the "Great Attractor" is ~4200 km s^{-1} in the Local Group reference frame, in good agreement with the conclusions of Lynden-Bell *et al.* (1987), who fitted a fairly similar model to a sample of elliptical galaxies.

A problem with both this model and that of Lynden-Bell *et al.* is that the direction of v_{LG} is 30° away from that of the microwave dipole anisotropy, v_{CMB}. The present data do not constrain the problem strongly enough to solve simultaneously for the distance and direction of the second mass concentration. Indeed, even the present solution for r_{GA} shows a strong dependence on the weakest data in the sample, namely the distance of Cen 45. It will be necessary to measure the peculiar velocities of clusters behind the "Great Attractor" to achieve this goal. The properties of some of these models are summarized in Table 9. Note that model 6, in which $w_j \equiv v_{CMB} - w_i$ (with one free parameter, w_i), has $\chi^2/N = 1.8$.

We hasten to add a number of disclaimers in respect of the linear bi-infall model. In this parameterized model we have optimized a simple dynamical representation in order to find the best fit to the available data subject to the constraint that the model also predict the size of the microwave dipole anisotropy. That does not mean that the model is a satisfactory or unique description of the general mass distribution inside 100 Mpc or that a linear spherical model is appropriate close to Virgo or to the second mass concentration. Furthermore, although the model is a dynamical one, it actually has a larger χ^2 than the simplest kinematic model which can be fitted to the data in Table 8, in which only the observer is moving in the CMB frame. This "null model" (model 9 in Table 9) would not

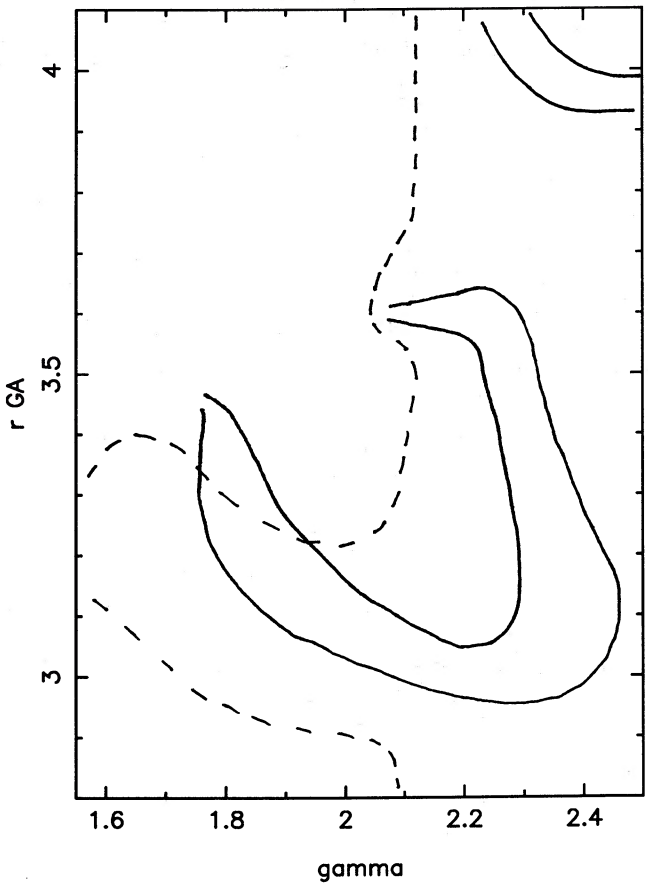

FIG. 8.—Two of the four parameters of the linear bi-infall model are r_{GA}, the distance of the second mass concentration in units of the distance to Virgo and γ, the index of the power-law density fall off. The dashed line separates the low χ^2 area on the left from the $\chi^2/N > 1.4$ area to the right in this parameter space. The central area (almost) enclosed by the solid contours contains the parameter space of $550 < v_{LG} < 650$ km s^{-1}. Best fits of the model also yielding acceptable values of v_{LG} are in the vicinity of $r_{GA} = 3.4$ and $\gamma = 1.8$.

[16] Hence we are solving for all four parameters simultaneously, but *assuming* the direction of the Great Attractor. A detailed comparison of models and fitting procedures here and in Lynden-Bell *et al.* (1987) is beyond the scope of this paper.

TABLE 9

THE LINEAR BI-INFALL MODEL

No.	Sample	v_{Virgo}	r_{GA}	γ	w_i	±	w_j	±	χ^2/N	v_{rms}	$v_{LG} \cdot \hat{v}_{CMB}$	v_{LG}	v_{GA}
1	Table 8	1073	3.3	1.8	240	37	486	60	1.39	338	527	621	4122
2	Table 8	1073	3.56	1.69	241	38	577	56	1.36	335	596	707	4319
3	E gals		[a]	[a]	≡100		570	60	≡1.00		615	705	4350
4	Arecibo	1073	3.2	2	194	23	504	60	0.63	354	510	607	4006
6	Table 8	1073	3.4	1.85	285	60	455		1.8	437	≡600	≡600	4378
7	Table 8		[b]	[b]					1.26	310	500	610	
8	Table 8	1020	3.3	1.8	287	32	514	67	1.50	351	580	680	4064
9	Table 8		[c]	[c]					0.56	220	369	541	

[a] The Great Attractor model of Lynden-Bell *et al.* 1987.
[b] Self-consistent model of Yahil 1988.
[c] Null model (see text).

be an acceptable fit to IRTF data in the Local Supercluster, however. From these data Aaronson *et al.* (1982) found $w_i = 250 \pm 64$ km s^{-1}, which is fully consistent with model 1.

To conclude, Figure 9 is a contour map of the velocity field corresponding to model 1. It represents the data smoothly, but it is not necessarily an accurate picture of this complex region. A qualitative description which emphasizes the hard observational facts may even be preferable. What we have observed is a number of groups of spiral galaxies mostly in the foreground of major mass concentrations in Hydra and Centaurus. The observed positive peculiar velocities of the spirals in Antlia, ESO 508, Pavo, and an undetermined portion of Centaurus are due to their acceleration into these mass concentrations.

X. A SELF-CONSISTENT MODEL OF THE GRAVITATIONAL FIELD

Discovery of the Virgocentric flow accounted for part of the microwave dipole anisotropy, but left 75% of the Local Group motion unexplained. Introduction of a second simple mass concentration has reduced the residual to 55%. The road to further success in understanding our motion as observers and describing kinematics locally is therefore clear. A satisfactory model will need to incorporate the full complexity of the gravi-

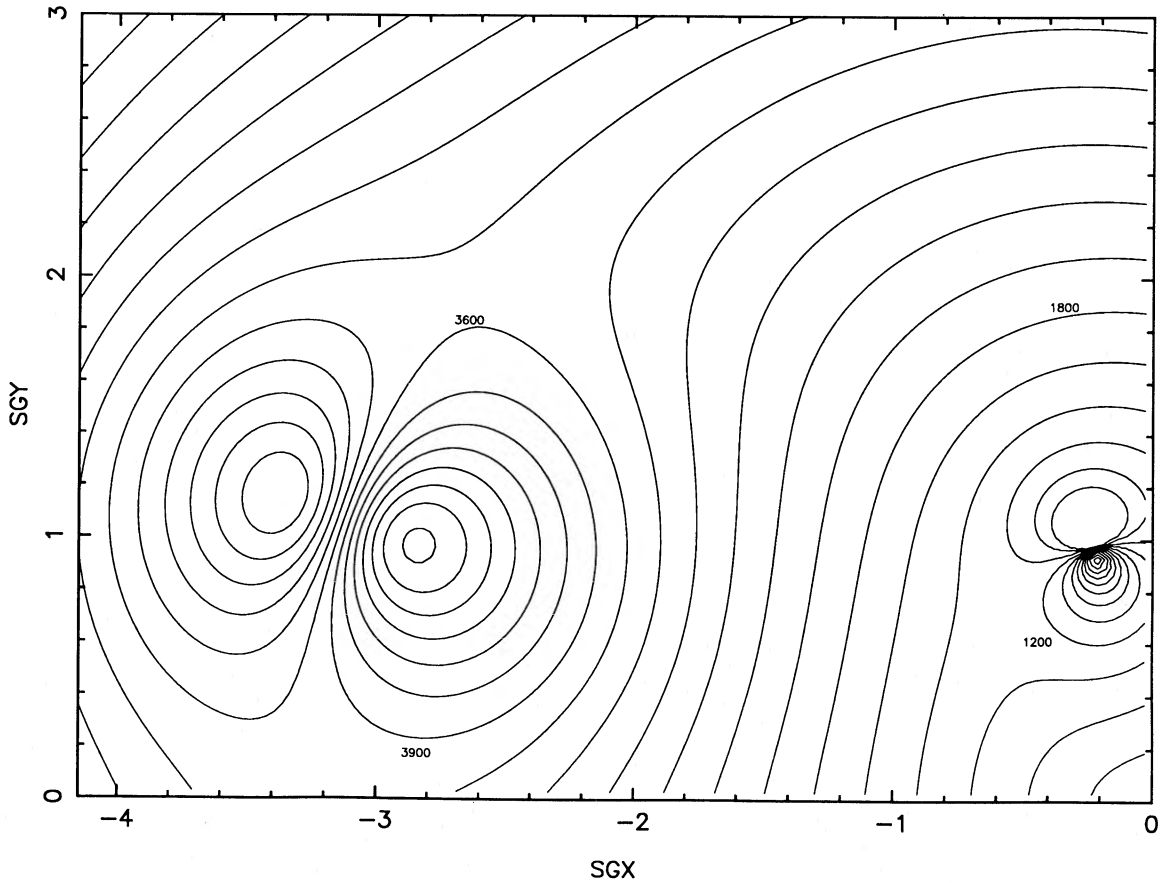

FIG. 9.—Contours of constant observed velocity referred to the Local Group in the second quadrant of the supergalactic plane. The unit of distance is the distance to Virgo which is close to SGY = 1, SGX = −0.2. The "Great Attractor" is seen near SGY = 1, SGX = −3.3. The contour interval is 300 km s^{-1} and the model parameters are those of model 1 in Table 9.

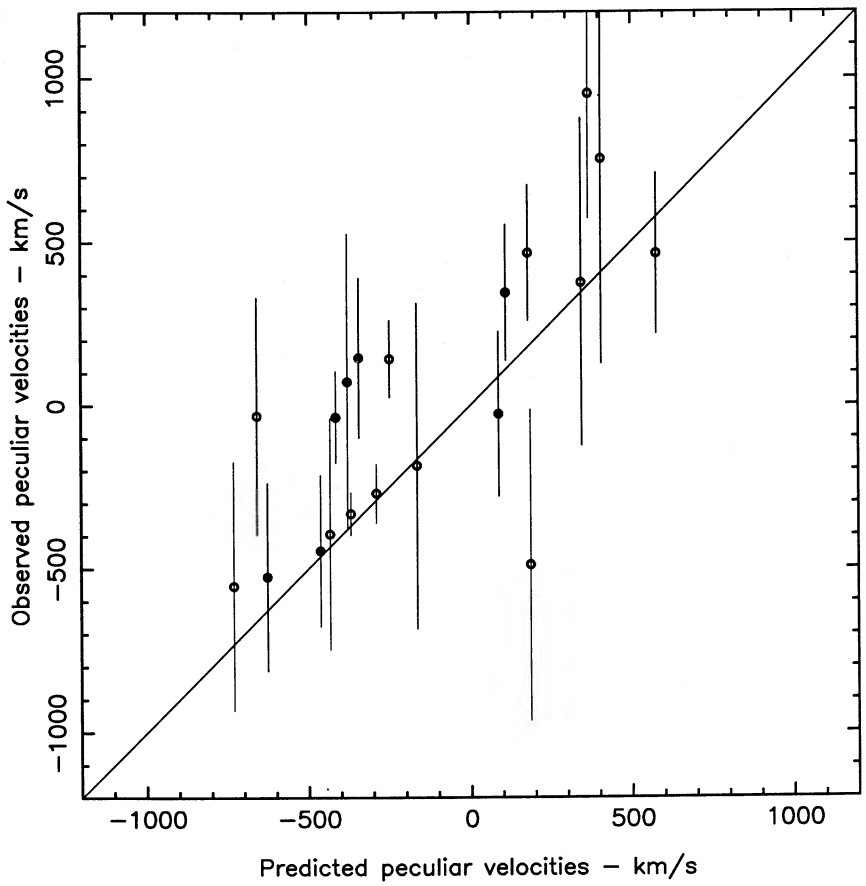

FIG. 10.—Observed peculiar velocities in the reference frame of the Local Group vs. peculiar velocities predicted from the gravitational field constructed by Yahil (1988). The filled symbols are the Parkes clusters, the open symbols the Arecibo clusters.

tational field within 100 Mpc. A pioneering treatment of this problem has been undertaken by Strauss and Davis (1988*a*) and Yahil (1988). Their model employs an iterative derivation of the redshift-distance relation to arrive at a self-consistent description of the gravitational field based on a complete redshift survey of *IRAS* galaxies. In this model there is in principle one free parameter: Ω, the ratio of the overall density to the critical density. As with the bi-infall model, the linear approximation for velocity perturbations is employed.

Figure 10 offers a comparison of the observed peculiar velocities of our clusters with the predicted values of v_{pec} from this model. These were kindly provided by Amos Yahil prior to publication and are calculated in the rest frame of the Local Group from a model with $\Omega = 0.5$. The agreement in general seems to be good; the most significant disagreements are in the high observed peculiar velocities of Antlia and the ESO 508 group and also of the Fornax Cluster. The value of χ^2 and the rms difference between the observed and predicted cluster velocities for this model are lower than model 1 in Table 9. (In computing χ^2 we substituted $\partial v/\partial r = H_0$ in eq. [1].)

This class of self-consistent model seems very promising for the study of the local velocity field, although the current model's predicted direction of motion of the Local Group is still 20° to 25° from the microwave dipole anisotropy (Strauss and Davis 1988*b*)

XI. PECULIAR VELOCITIES COMPARED WITH EXPECTATIONS FROM THEORY

The distribution of peculiar velocities in the 20 cluster sample of Table 8 is shown in Figure 11*a*. Also shown is the expectation from the individual observational errors in redshift and distance assuming Gaussian statistics. In the total sample the occurrence of positive peculiar velocities larger than 400 km s^{-1} seems to exceed what would be expected if an experiment were conducted with these measuring errors.

If we were to compare these measurements with the predictions of a theory in which the source of peculiar velocities was gravitational, we would expect that in a fair sample of the universe as many negative as positive peculiar velocities would be observed, and the folding of the data carried out in Figure 11*b* would be a better basis for comparison. Now the excess of large peculiar velocities over the error distribution seems less convincing.

We can probably best understand the fact that in the Arecibo sample of clusters Aaronson *et al.* (1986) did not see peculiar velocities larger than the statistical errors, but that the Parkes sample contains some examples of significant peculiar velocities, if we suppose that in the Parkes sample we are seeing the tail of a distribution of peculiar velocities, whose rms value in a large sample is of the same order as the statistical errors. In

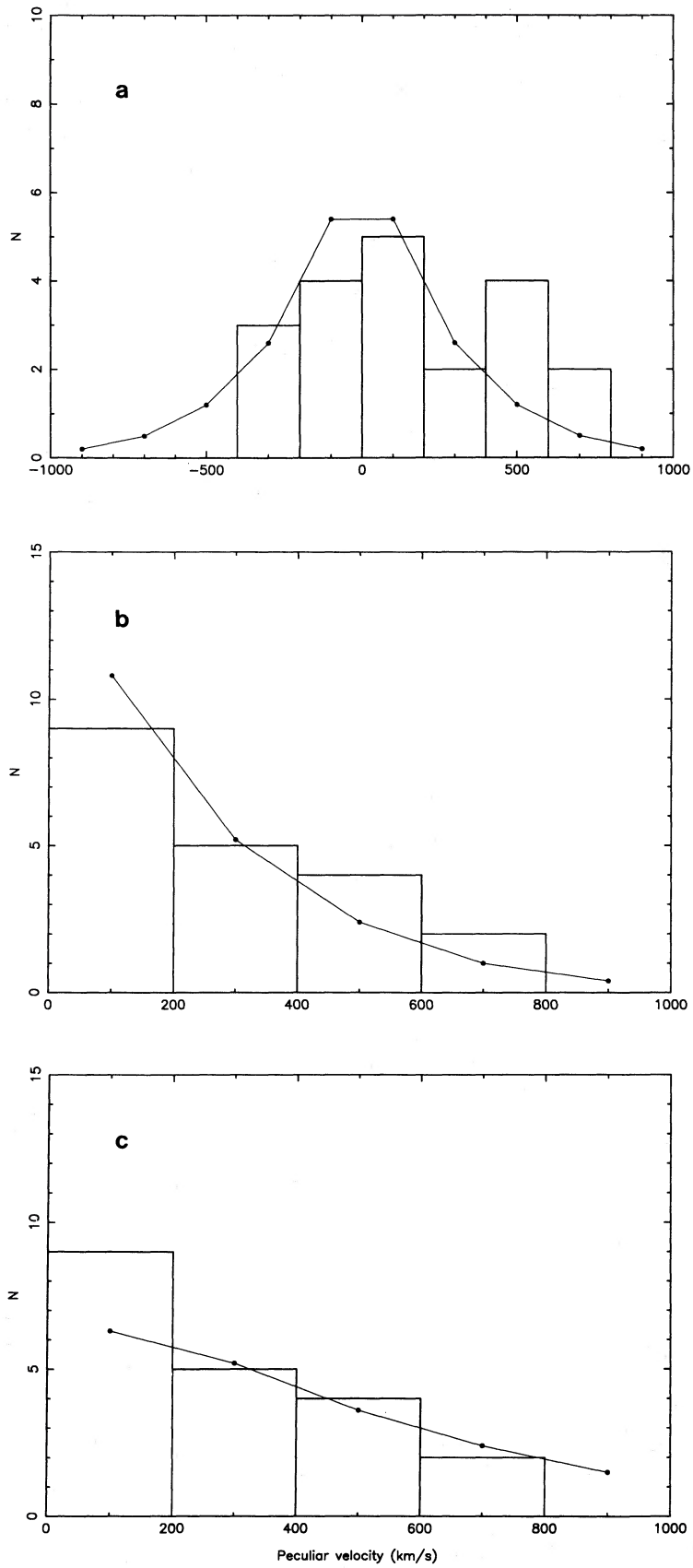

FIG. 11 (*a*) (*top*).—The histogram is the distribution of peculiar velocities in the CMB frame for the sample in Table 8. The linked points indicate the distribution expected from the statistical errors in the table. A significant excess of positive peculiar velocities is seen. (*b*) (*center*). The data are rebinned into $|v_{pec}|$. The excess of large peculiar velocities no longer seems so significant. (*c*) (*bottom*). The histogram is the same as in (*b*); the statistical errors have been broadened by $v_{pec}(\text{rms}) = 400$ km s^{-1}. The broadened distribution has an excess of large peculiar velocities and a deficiency of small ones.

fact the skewness of Figure 11*a* (which is not seen in the distribution for the Arecibo sample[17]) results from the concentration of the Parkes sample on the nearside of the Great Attractor region. It seems best to use the observed distribution in Figure 11 to put an upper limit on v_{pec}(rms). Figure 11*c* compares the observed distribution with the error distribution broadened by 400 km s^{-1}. The data are consistent with v_{pec}(rms) < 400 km s^{-1}.

The confidence level to be attached to this upper limit can be estimated in two ways. First a Monte Carlo calculation can be performed in which the likelihood of events in the first and beyond the fourth bins of Figure 11*c* are compared. Second, Kolmogorov-Smirnov statistics reject the hypothesis that the data can be represented by a one-sided Gaussian with $\sigma > 510$ km s^{-1}. The error distribution when folded with $\sigma = 400$ km s^{-1} resembles a Gaussian with $\sigma = 525$ km s^{-1}. Both tests yield v_{pec}(rms) < 400 km s^{-1} at the 95% confidence level.

Our clusters are defined in terms of radii of 4° at 3000 km s^{-1} redshift to 3° at 10,000 km s^{-1}, which is a range of 2 h^{-1} to 5 h^{-1} Mpc. We have seen, however, that in some cases a radius of 15 h^{-1} Mpc might be required to contain subgroups in the radial direction. We will consider the predictions of models for sphere of radius 5 h^{-1} Mpc, although clearly more detailed modeling is called for.

The hot dark matter (neutrino) model with 1-dimensional rms peculiar velocities on this scale of 1040 km s^{-1} (Vittorio, Juszkiewicz, and Davis 1986) is certainly inconsistent with the limits from Figure 11. However, stronger constraints on this model are imposed by the isotropy of the microwave background radiation (Readhead *et al.* 1988) on arcminute scales, and seem to rule out this model unequivocally.

Cold dark matter (CDM) models offer predictions which are more compatible with the present results. For the $\Omega = 1$ CDM universe rms peculiar velocities of 276 km s^{-1} are calculated on 5 h^{-1} Mpc scales by Vittorio, Juszkiewicz, and Davis. This value was obtained with $H_0 = 50$ km s^{-1} Mpc^{-1}, and would decrease approximately as $h^{-0.5}$ for larger H_0. Both these and the biased CDM models, whose v_{pec}(rms) is lower, satisfy the constraint from our statistics of peculiar velocities. The large coherence length and bulk flow velocity which could be attributed to a Virgo-Hydra-Centaurus supercluster (see § VIII) might also be compatible with these models. For a sphere of radius 25 h^{-1} Mpc in a CDM model, Vittorio (1986) has calculated an rms peculiar velocity of 156 $\Omega_0{}^{-0.18}$ $h^{-0.78}$ km s^{-1}, uncomfortably, but not critically, smaller than the value of 275 ± 135 km s^{-1} found in § VIII.

XII. CONCLUSIONS

1. Distances from the IRTF relation have been measured for six clusters of galaxies in the Hydra-Centaurus Supercluster.

2. Three of these clusters—Antlia, ESO 508, and Pavo—show significant (at the 2 σ level) positive peculiar velocities of order 500 km s^{-1} in a comoving reference frame in which the observer is at rest with respect to the CMB radiation. The principal component of the Centaurus Cluster also has a similar peculiar velocity.

3. There are significant discrepancies in a comparison of relative distances between the present spiral samples and elliptical samples nominally in the same clusters. This is probably due to substructure in the Hydra-Centaurus Supercluster complex. But further work is required to rule out any systematic differences between northern and southern hemisphere samples of spirals and ellipticals.

4. The net peculiar velocity of the sample suggests that Hydra-Centaurus tends to share the motion of the Local Group in this CMB reference frame. Taken as a whole, Virgo-Hydra-Centaurus has a peculiar velocity of 275 ± 135 km s^{-1}. This is smaller in both coherence length and amplitude than was reported for elliptical galaxies in the same volume by Dressler *et al.* (1987).

5. When added to the Arecibo cluster sample, the data also fit a model in which two mass concentrations, one at Virgo and one just beyond the centroid of the Parkes sample, perturb the Hubble flow. If the model is also required to satisfy the condition $v_{LG} = 600 \pm 50$ km s^{-1}, the local infall velocities toward these two centers are 240 ± 37 and 486 ± 60 km s^{-1}, respectively.

6. A model by A. Yahil of the full gravitational field in the sample volume provides a better fit to the data without requiring a mass distribution different from the distribution of galaxies. Such models seem to provide the best basis for improving our description of the kinematics of galaxies locally, and eventually constraining the global density parameter.

7. Despite the significance of the peculiar velocities of some clusters, the present sample can put an upper limit only on the rms peculiar velocities in the population of gravitationally perturbed clusters from which the present sample is drawn. This upper limit is v_{pec}(rms) < 400 km s^{-1} at the 95% confidence level and refers to scales of order 5 h^{-1} Mpc.

8. These measurements of peculiar velocities remain consistent with the expectations for a CDM dominated universe, although the 45 h^{-1} Mpc coherence length of the Virgo-Hydra-Centaurus flow is an uncomfortable constraint.

The best qualitative summary of the present state of this work is provided by Figure 7. Study of Figure 7 suggests the following questions.

a. Are the unobserved clusters in Hydra-Centaurus participating in the large-scale flow, or are they at rest like Hydra?

b. If gravity is the source of the flow and the "Great Attractor" the center, do galaxies as far behind Hydra-Centaurus as the Local Group is in front have peculiar velocities of −600 km s^{-1}.

c. If not, could the explosive models of Ostriker (1986) possibly fit the data?

d. Does the Perseus-Pisces Supercluster exhibit peculiar velocities of similar size, as the *IRAS* survey models predict?

These questions must await further work. Further tuning of the Tully-Fisher relation along the lines attempted by Bothun and Mould (1987) and the existence of the complementary Faber-Jackson relation for ellipticals offer hope that a good deal more can be learned about the distribution of peculiar velocities on large scales.

We owe a great debt to Eric Persson who built the IR photometers for Las Campanas Observatory and helped with the first observations. We also wish to thank Kent Budge, Oscar Duhalde, and James Schombert for their assistance. Partial support for this project was provided by NSF grants AST 83-16629 and 86-11405 to the University of Arizona plus AST

[17] The symmetry of this distribution for the Arecibo sample was the basis for the conclusion by Aaronson *et al.* (1986) that the microwave dipole anisotropy arises locally.

85-02518 and 87-21705 to Caltech. The Aspen Center for Physics offered hospitality and useful interactions during the final drafting of this paper. His co-authors wish to remember Marc Aaronson who died at Kitt Peak just two months after the conclusion of the key observing run at Parkes reported here. This paper is one of his many memorials.

REFERENCES

Aaronson, M. Bothun, G., Budge, K., Dawe, Dickens, R., Hall, P., Lucey, J., Mould, J., Murray, J., Schommer, R., and Wright, A. 1987, *Large Scale Structure in the Universe*, ed. J. Audouze and A. Szalay (Dordrecht: Reidel), p. 185.
Aaronson, M., Bothun, G., Mould, J., Huchra, J., Schommer, R., and Cornell, M. 1986, *Ap. J.*, **302**, 536.
Aaronson, M., Dawe, J., Dickens, R., Mould, J., and Murray, J. 1981, *M.N.R.A.S.*, **195**, 1P.
Aaronson, M., Huchra, J., and Mould, J. 1979, *Ap. J.*, **229**, 1.
Aaronson, M., Huchra, J., and Mould, J., Schechter, P. L., and Tully, R. B. 1982, *Ap. J.*, **258**, 64.
Aaronson, M., *et al.* 1982, *Ap. J. Suppl.*, **50**, 241.
Aaronson, M., and Mould, J. 1983, *Ap. J.*, **265**, 1.
———. 1986, *Ap. J.*, **303**, 1.
Aaronson, M., Mould, J., and Huchra, J. 1980, *Ap. J.*, **237**, 655.
Aaronson, M., Mould, J., Huchra, J., Sullivan, W. T., Schommer, R. A. and Bothun, G. D. 1980, *Ap. J.*, **239**, 12.
Ables, J. G., Cooper, B., Hunt, A., Moorey, G., and Brooks, J. 1975, *Rev. Sci. Instrum.*, **46**, 284.
Bothun, G., Aaronson, M., Schommer, R., Mould, J., Huchra, J., and Sullivan, W. 1985, *Ap. J. Suppl.*, **57**, 423.
Bothun, G. and Mould, J. 1987, *Ap. J.*, **313**, 629.
Burstein, D., Davies, R., Dressler, A., Faber, S., Stone, R., Lynden-Bell, D., Terlevich, R., and Wegner, G. 1987, *Ap. J. Suppl.*, **64**, 601.
Cornell, M., Aaronson, M., Bothun, G., Mould, J., Huchra, J., and Schommer, R., 1987, *Ap. J. Suppl.*, **64**, 507.
Davies, R., Burstein, D., Dressler, A., Faber, S., Lynden-Bell, D., Terlevich, R., and Wegner, G. 1987, *Ap. J. Suppl.*, **64**, 581.
Davis, M., and Peebles, J. 1983, *Ann. Rev. Astr. Ap.*, **21**, 109.
de Vaucouleurs, G., de Vaucouleurs, A., and Corwin, H. 1976, *Second Reference Catalogue of Bright Galaxies* (Austin: University of Texas Press) (RC2).
Dickens, R. Currie, M., and Lucey, J. 1986, *M.N.R.A.S.*, **220**, 679.
Dressler, A. 1988*a*, *Sci. American*, **257**, 46.
———. 1988*b*, *Ap. J.*, **329**, 519.
Dressler, A., Faber, S., Burstein, D., Davies, R., Lynden-Bell, D., Terlevich, R., and Wegner, G. 1987, *Ap. J. (Letters)*, **313**, L37.
Faber, S. M., Wegner, G., Burstein, D., Davies, R., Dressler, A., Lynden-Bell, D., and Terlevich, R. 1988, preprint.
Fisher, J. R., and Tully, R. B. 1981, *Ap. J. Suppl.*, **47**, 139.
Fixsen, D. J., Cheng, E. S., and Wilkinson, D. T. 1983, *Phys. Rev. Letters*, **50**, 620.
Geller, M., and Huchra, J. 1982, *Ap. J. Suppl.*, **52**, 61.
Hopp, U., and Materne, J. 1985, *Astr. Ap. Suppl.*, **61**, 93.
Han Ming Sheng, and Mould, J. R. 1988, in preparation.
Huchra, J. P. 1988, in preparation.
Kraan Korteweg, R. C. 1986, *Astr. Ap.*, **66**, 255.
Lauberts, A. 1982, *The ESO/Uppsala Survey of the ESO (B) Atlas* (Munich: European Southern Observatory).
Lubin, P. M., Epstein, G. L., and Smoot, G. F. 1983, *Phys. Rev. Letters*, **50**, 616.
Lucey, J., and Carter, D. 1988, preprint.
Lucey, J., Currie, M., and Dickens, R. 1986*a*, *M.N.R.A.S.*, **221**, 453.
———. 1986*b*, *M.N.R.A.S.*, **222**, 427.
Lynden-Bell, D., Faber, S., Burstein, D., Davies, R., Dressler, A., Terlevich, R., and Wegner, G. 1988, *Ap. J.*, **326**, 19.
Mould, J., and Ziebell, D. 1982, *Pub. A.S.P.*, **94**, 221.
Nilson, P. 1973, *Uppsala General Catalogue of Galaxies* (*Uppsala Astr. Obs. Ann.*, Vol. **6**) (UGC).
Ostriker, J. P. 1986, in *Galaxy Distances and Deviations from Universal Expansion*, ed. B. F. Madore and R. B. Tully (Dordrecht: Reidel), p. 273.
Peebles, P. J. E. 1976, *Ap. J.*, **205**, 318.
Readhead, A. C. S., Lawrence, C., Myers, S. T., Sargent, W. L. W. S., Hardebeck, H. E., and Moffet, A. T. 1988, preprint.
Richter, O. G., and Huchtmeier, W. K. 1987, *Astr. Ap. Suppl.*, **68**, 430.
Sandage, A. 1975, *Ap. J.*, **202**, 563.
Schechter, P. L. 1980, *A.J.*, **85**, 801.
Shaya, E. J. 1984, *Ap. J.*, **280**, 470.
Strauss, M. A., and Davis, M. 1988*a*, *Pont. Acad. Sci. Scripta Varia*, in press.
Strauss, M. A., and Davis, M. 1988*b*, private communication.
Tammann, G., and Sandage, A. 1985, *Ap. J.*, **294**, 81.
Tonry, J. M., and Davis, M. 1981, *Ap. J.*, **246**, 680.
Tully, R. B., and Fisher, J. R. 1987, *Nearby Galaxies Atlas* (Cambridge: Cambridge University Press).
Vittorio, N. 1986, in *Galaxy Distances and Deviations from Universal Expansion*, ed. B. F. Madore and R. B. Tully (Dordrecht: Reidel), p. 251.
Vittorio, N., Juszkiewicz, R., and Davis, M. 1986, *Nature*, **323**, 132.
Whitmore, B., Forbes, D., and Rubin, V. 1988, *Ap. J.*, **333**, 542.
Yahil, A. 1988, *Pont. Acad. Sci. Scripta Varia*, in press.

MARC AARONSON: deceased.

GREG BOTHUN: Astronomy Department, University of Michigan, Ann Arbor, MI 48109

MARK CORNELL: Steward Observatory, University of Arizona, Tucson, AZ 85721

JOHN DAWE: Siding Spring Observatory, Coonabarabran, NSW 2357, Australia

R. J. DICKENS: Rutherford Laboratory, Chilton, Didcot, Oxfordshire OX11 0QX, England

PETER HALL: School of Electrical Engineering, University of Sydney, Sydney, NSW 2006, Australia

HAN MING SHENG and JEREMY MOULD: Caltech 105-24, Pasadena CA 91125

JOHN HUCHRA: Center for Astrophysics, 60 Garden St., Cambridge, MA 02138

JOHN LUCEY: Department of Physics, University of Durham, South Road, Durham DH1 3LE, England

JOHN MURRAY: CSIRO Division of Radiophysics, P.O. Box 76, Epping, NSW 2121, Australia

ROBERT SCHOMMER: Department of Physics and Astronomy, Rutgers University, P.O. Box 849, Piscataway, NJ 08854

ALAN WRIGHT, ANRAO, P.O. Box 276, Parkes, NSW 2870, Australia